CHALMERS

Vertically aligned carbon nanofiber synthesis on top of TiN films for NEMS devices

Thesis for the Degree of Master of Science in Biomedical Engineering

MARIA ELENA LOPEZ DAMIAN

Department of Microtechnology and Nanoscience

CHALMERS UNIVERSITY OF TECHNOLOGY

Göteborg, Sweden, 2011

Vertically aligned carbon nanofiber synthesis on top of TiN films for NEMS devices

María Elena López Damián

Department of Microtechnology and Nanoscience
CHALMERS UNIVERSITY OF TECHNOLOGY
Göteborg, Sweden, 2011

Title: Vertically aligned carbon nanofiber synthesis on top of TiN films for NEMS devices

© María Elena López Damián

Supervisor & Examiner: Dr. Per Lundgren

Chalmers University of Technology

Sweden

Supervisor: Farzan Alavian Ghavanini

Chalmers University of Technology

Sweden

Department of Microtechnology and Nanoscience

Göteborg, Sweden 2011

Abstract

Plasma enhanced chemical vapour deposition is used for the synthesis of vertically aligned carbon nanofibers from Ni catalyst particles deposited by hole mask colloidal lithography on top of TiN. The TiN underlayer is reactively sputtered in a reliable and repeatable manner. TiN has been selected for its CMOS compatibility and good performance as a diffusion barrier having in mind the aim of using the carbon nanofibers for nanoelectromechanical devices (NEMS). The optimal growth conditions for the carbon nanofibers are estimated from annealing, growth temperature, gas ratio, power and pressure parameter study. The characterization of the as deposited carbon nanofibers is performed by scanning and transmission electron microscopy techniques. A growth mechanism is proposed where a carbon deposit free catalyst surface sustained during the whole synthesis results in a carbon diffusion limited growth. If the balance between the carbon bearing species and the etching agents is distorted in favor of carbon formation the growth will shift to a carbon supply-limited process instead. Transitions between aligned tip type and unaligned base type fibers are explained in terms of the dominant process at the initial phase of the growth. The growth mode will be defined by the first graphene layers site of formation being either the catalyst or the catalyst-substrate interface.

List of appended papers

I. **Growth characterization of vertically aligned carbon nanofibers on top of TiN buffer layer for nanoelectromechanical devices.**
F. Alavian Ghavanini, M. Damian, D. Rafieian, P. Lundgren.
Procedia Engineering, 24th Eurosensors Conference Linz, Austria, Sep 05-08, 2010. 5 s. 1115-1118.

II. **Controlling the initial phase of PECVD growth of vertically aligned carbon nanofibers on TiN.**
F. Alavian Ghavanini, M. Lopez-Damian, D. Rafieian, K. Svensson, P. Lundgren and P. Enoksson (in press).
Sensors and Actuators A: Phys, 2011,doi:10.1016/j.sna.2011.04.036

Contents

1. Introduction 1

2. Fundamentals of Carbon Nanostructures 3

2.1 Structure 3

2.2 Properties 6

2.3 Synthesis 6

2.3.1 Arc Discharge 7

2.3.2 Laser Ablation 7

2.3.3 Catalytic Chemical Vapor Deposition 7

2.3.4 Catalytic Plasma Enhanced Chemical Vapor Deposition 8

3. DC-PECVD 9

3.1 Plasma Sheath Distribution 10

3.2 Plasma Chemistry 11

3.3 Growth Mechanism of CNF 12

3.4 Plasma Chemistry in the Synthesis of CNF from C_2H_2 and NH_3 precursors 13

3.5 PECVD Reactor for Growth Study 14

4. VACNF Catalyst Patterning and Growth Sequence 16

4.1 Substrate Preparation 16

4.2 Growth Sequence 19

5. Results 21

5.1 Annealing Treatment 21

5.2 Plasma Pretreatment 22

5.3 Oxygen Plasma Treatment on TiN 23
5.4 Growth Parameters Effect 24
5.4.1 Growth Temperature 24
5.4.3 Gas Pressure 25
5.4.4 Gas Ratio 26
5.5 Growth Repeatability 27
5.5 Growth Mechanism 29
5.6 VACNF Growth Optimization 32
6. Conclusions 35
7. References 39

1. Introduction

The great success of the microelectronic technology relies on its ability to integrate a huge number of devices in a single silicon chip making electronic systems smaller, more efficient and less power dissipative. The electronic component density within a single chip was roughly doubled every 2 years for more than four decades after predicted by Gordon Moore in 1965[1] prediction known as the Moore´s law. However, difficulties to continue with this trend have been acknowledged. Nowadays, the size of the node technology (gate length) for a commercial transistor is 32 nm further reductions are increasingly difficult to achieve mainly due to the complexity and cost of the involved fabrication processes and issues associated with the low dimensional scales.

Currently, the microelectronic components are fabricated following a top-down approach based on lithographic methods. The smallest device achievable with this technique is limited by the wavelength of the radiation used to expose the resist. Electron beams and deep ultraviolet (DUV) radiation make it possible to routinely produce features down to 50 nm in a cost effective manner; infrastructure required for feature sizes in the order of 20 nm and less (extreme UV for example) become prohibitively expensive and slow, therefore continuous improvements or new fabrication methods should be pursued.

However, when nanoscale dimensions are reached, materials experience changes in their physical properties as quantum effects start to dominate. For instance, nanotransistors will show stress induced leakage currents, loss of oxide insulating properties due to quantum tunneling current effects, semiconductor statistical doping fluctuations, interconnect voids from high current flows and increases in power dissipation[1].

Nanoscience and nanotechnology have emerged as solutions to designing and implementing new materials and components within the 1-100 nm scale. Carbon nanostructured materials such as carbon nanotubes, CNTs, and carbon nanofibers, CNFs, have received substantial attention as possible candidates to overcome the obstacles of current technology. They exhibit excellent physical and mechanical properties, in most of the cases better than currently used materials, and their synthesis is performed by a bottom-up approach where single molecules assemble themselves to form their structure. By using this approach it is possible to control the feature size dimension at few nm or even atomic scale.

As mentioned before, the continuous effort in carbon nanostructures (CNS) research is motivated to a large extent by the expected commercial applications. CNS are attractive for a wide variety of technological solutions ranging from strong and light composite materials[2,3] to nanoelectromechanical systems (NEMS)[4,5] , the latter being the main area of interest of this work.

Carbon nanotubes have proven to be useful in memory devices[6], resonators[7], sensors[8] and switches[9]. In these applications CNTs are normally placed parallel to the substrate in the desired configuration after being synthesized elsewhere. Their inherent synthesis conditions (i.e. high growth temperature) make it hard to grow them directly on top of the functional device limiting their feasibility to be integrated to some NEMS devices. Vertically aligned carbon nanofibers constitute an alternative to overcome this problem. The location, alignment and morphology of the fibers can be controlled during their synthesis therefore facilitating their use as building block for NEMS.

The aim of this work is to optimize the synthesis of vertically aligned carbon nanofibers (VACNFs) by a commercially available direct-current plasma enhanced chemical vapor deposition equipment named Black Magic II. The VACNFs are intended for the development of NEMS devices; as a result they should be both mechanically independent from each other and connected to a conducting electrode to be used as individual functional elements. The quality of VACNFs and the electrical properties of the electrodes will define the performance of the device. Materials that are commonly used in CMOS technology as conductive electrodes such as cooper seem to jeopardize the synthesis of the VACNFs. A possible solution to this problem is the use of a diffusion barrier between the catalyst and the electrode material that could inhibit their interaction during the CNF synthesis. Titanium nitride (TiN) is a conductive material with good stability at high temperatures so it can be used in the PECVD process. Besides, its compatibility to both VACNFs and CMOS makes it a good candidate for further integration of the VACNFs based NEMS to IC technology. Therefore, VACNFs were synthesized on top of $Si/SiO_2/TiN$ substrates with pre-deposited nickel catalyst dots.

Hole mask colloidal lithography was adopted to pattern the catalyst dots on the substrates due to its feasibility for growth optimization studies. For instance, it is not as expensive as the other techniques such as e-beam lithography, it has a high throughput, the colloidal particles determine the smallest feature size and several pattern geometries can be obtained with process modifications.

This thesis is structured in 5 chapters. The *Fundamentals of carbon nanostructures* chapter provides a general insight into carbon nanostructures for those who are not familiar with this field. Chapter 3 provides a description of the PECVD deposition process and of the equipment used in this work. In Chapter 4, the sample preparation and the growth method are explained. In chapter 5, the results and discussions are presented along with future work suggestions. Finally, chapter 6 gives the general conclusions of the present work.

2. Fundamentals of Carbon Nanostructures

2.1 Structure

Carbon is one of the most versatile elements in nature because it can form multiple bonds, chains, and rings when connected to other carbon atoms or molecules. The hybridization of its 4 valence shell electrons results in different mechanical and electrical properties for its allotropes even though their constituent is identical. Pure carbon based allotropes are based on sp^2 or sp^3 orbital hybridizations. Sp^3 hybridization gives diamond its great hardness in contrast to sp^2 hybridization which provides graphite with its softness.

Graphite is formed by several graphene sheets made of carbon atoms covalently bonded in hexagonal networks. Different layers are weakly bound by van der Waals forces giving to the entire structure an anisotropic character with in plane stability and normal to plane instability. If one of these graphene layers is detached from the bulk material and then rolled up to form a cylinder we would obtain a carbon nanotube. Depending on the direction the graphene sheet is rolled, the CNT will have a different structure and therefore different electrical properties. There are three different ways to roll the graphene sheet described in terms of the chiral vector (C_h) shown in Figure 1.

$$\underline{C}_h = n\underline{a}_1 + m\underline{a}_2$$

Both integers n and m and the directions given by the unit cell base vectors of a graphene sheet (a_1 and a_2) define the rotation around the tube axis (T) of the point (n,m) onto the origin (0,0). From m and n values CNTs are named armchair when n=m, zigzag if n=0 or m=0 and chiral in the case of $m \neq n \neq 0$.

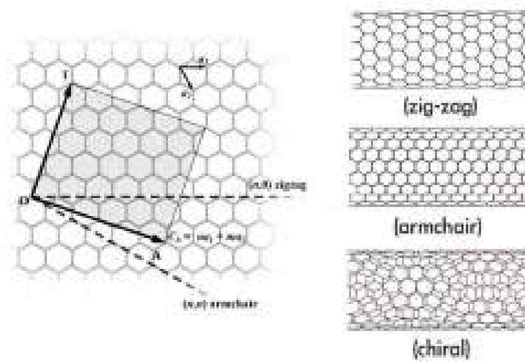

Figure 1. Left: chiral vector, Ch, definition. Right: types of CNTs based on their chirality[10].

Each (n,m) pair corresponds to a specific chiral angle, φ, and diameter, d:

$$\varphi = \arccos\left[\sqrt{3}(n+m)/(2\sqrt{(n^2+m^2+nm)})\right] \qquad d = a/\pi \cdot \left[\sqrt{(n^2+m^2+nm)}\right]$$

Carbon nanotubes are also considered as carbon allotropes as they have graphite as their building block. They have a high aspect ratio with diameters ranging from 0.4 nm up to few nm and lengths up to hundreds of μm[11].

CNTs are classified as single wall carbon nanotubes (SWCNTs) and multiwall carbon nanotubes (MWCNTs), the former having only one graphene sheet and the latter formed by 2-50 concentrically stacked SWCNTs with inner and outer diameters of 1.5 to 15 nm and 3 to 50 nm respectively[11]. These concentric tubes are separated by the interlayer spacing in graphite of 0.34 nm. The angle (α) between the tube axis and the graphene sheet close to the sidewall equals zero as shown in Figure 2 (a). When $\alpha \neq 0$ the tubular structure becomes a carbon nanofiber shown in Figure 2 (b).

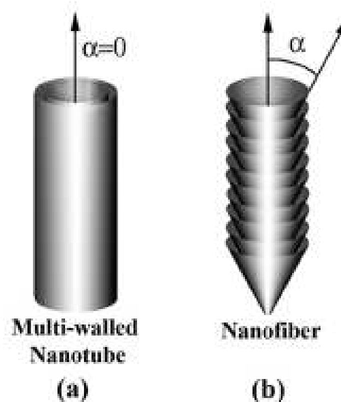

Figure 2. The difference in the angle (α) between the CNS axis and the graphene sheet near sidewall gives as a result two different carbon nanostructures (a) MWCNT and (b) CNF. Reprinted from [12] with the kind permission of Dr Anatoli Melechko. © 2007, American Institute of Physics.

Carbon nanofibers are commonly misclassified as MWCNTs since they are also formed by several sp^2 hybridized carbon atoms sheets. CNFs are made of curved graphite layers stacked as cones or cups. The stacked cup structure is called bamboo type CNF (Figure 3 left) while the stacked cone structure is denoted as herringbone or fishbone CNF (Figure 3 right); both types owe their name to their similarity in structure with the related object as seen in transmission electron microscope images.

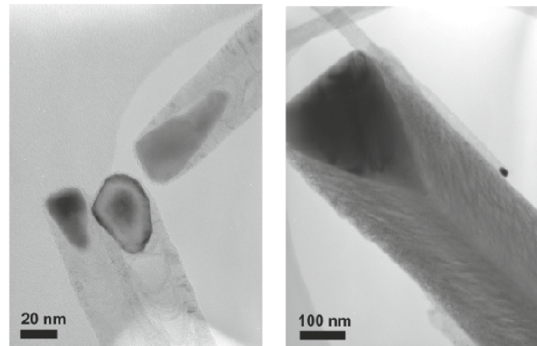

Figure 3. Left: A bamboo type CNF. Right: A herringbone CNF.

In contrast with the highly ordered structure of CNTs, CNFs have a disordered crystalline structure along the filament with many dangling bonds on their surface that most likely can be accessible for chemical or physical interactions such as adsorption. Research has been conducted in order to use CNFs for H_2 storage[13]. They also have a high aspect ratio ranging from tens to hundreds of nm in diameter and up to mm in length.

If the CNFs are grown perpendicular to the substrate they are called vertically aligned carbon nanofibers, VACNFs. Merkulov et al. demonstrated that the presence of the catalytic particle at the tip of the CNF is crucial for its vertical alignment[14]. This requirement can only be fulfilled by CNFs with tip growth mode (Figure 4 (right)) since base growth mode (Figure 4 (left)) is characterized by the capture of the catalyst at the bottom of the carbon fiber due to the strong contact adhesion between the catalyst and the substrate as well as the kinetic parameters during the synthesis which results in carbon filament bending during carbon deposition[15].

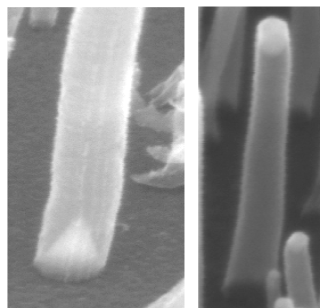

Figure 4- Left a base growth CNF where the catalyst remains attached to the substrate during deposition. Right: A tip growth CNF where the catalyst has been detached from the substrate during the deposition and remains at the tip of the fiber.

2.2 Properties

Graphene is a semiconductor with high electron mobility within plane but low electron mobility perpendicular to the plane because of its highly anisotropic properties. In the form of a nanotube it could exhibit semiconducting or metallic behavior depending on the boundary conditions defined by both its diameter and its chiral angle. CNTs with $(n - m)/3 \neq$ integer will be semiconducting having an energy gap of 20-50 meV[16] otherwise the tube will be metallic. For instance, all armchair tubes exhibit metallic behavior.

Since the walls are not parallel to the fiber axis in the case of CNFs, interplane electron mobility between the graphene layers instead of along the shell as in the case of CNTs result in higher resistivity values for CNFs. Zhang, L., et al., found that all the CNFs are metallic [17]. In addition to this, CNFs can withstand high current densities up to $1x10^7$ A/cm^2 [18] which could be used as a way to solve the interconnection breakage issues in current microtechnology devices.

CNTs possess extraordinary mechanical properties such as high mechanical strength, flexibility and ability to support compression without fracture. CNTs are the strongest man-made materials known with Young´s modulus values in the range of 2.8-3.6 TPa and 1.7-2.4 TPa for SWCNTs and MWCNTs respectively[19]. In the case of the CNFs the defects in their structure decrease their Young´s modulus to a value between 228 and 724 GPa[20]. Although a wide variety of composite materials have been implemented by taking into consideration this CNS feature, the fluctuations in the defect density of the carbon nanostructures limit their application to NEMS devices.

The CNFs structure is not altered if exposed to strong acids (e.g. HF), bases and solvents at room temperature making them a compatible material with CMOS technology[21,15]. The large active surface area provided by their dangling bonds at the borders renders them highly susceptible to surface functionalization and therefore suitable for biological applications.

2.3 Synthesis

The study of carbon nanostructures was originally initiated to prevent their formation in the process of hydrocarbon synthesis reactions [22]. It was the discovery of carbon nanotubes in 1991 by Iijima[23] which increased the interest of researchers in controlling the growth and tuning the carbon structure´s properties. Iijima used arc discharge deposition but nowadays laser ablation and catalytic chemical vapor deposition are also part of the techniques commonly employed in the production of these nanostructures.

2.3.1 Arc Discharge

Arc discharge can be used to produce large quantities of well-structured CNTs, CNFs and fullerenes. In a sub atmospheric pressurized chamber (50-700 mBar), a DC electric discharge arc is generated by applying a potential difference of some tens of volts between two graphite electrodes separated by a distance of few mm; the carbon in the anode is evaporated in a hot plasma and part of it condenses in the form of CNS deposits and soot on the cathode surface. Catalyst particles can be added to the electrodes to help in the synthesis of specific structures with a low concentration of defects. The length of the structures is limited to just few μm and exhibit random type and size distributions. In addition the synthesized CNSs are retrieved through a purification processes.

2.3.2 Laser Ablation

The technique is based on irradiating a target of graphite by using laser in an environment of controlled temperature and pressure in the presence of an inert gas (usually argon or helium). This process generates soot full of fullerenes, CNTs and CNFs that is carried by the gas injected and collected on a cool surface. The target can be modified to carry catalysts to help in the synthesis of the desired structure. The conditions of the process can be controlled to obtain structures of high crystalline quality. However, the random spatial distribution and the high cost of the lasers necessary to synthesize these structures prohibit mass production.

2.3.3 Catalytic Chemical Vapor Deposition

The catalytic chemical vapor deposition (C-CVD) process is based on the dissociation of hydrocarbon species on a substrate in the presence of a metallic catalyst which can be pre-deposited on top of the substrate or be derived from the pyrolysis of some organometallic compound in gaseous form. The hydrocarbons used as precursors can vary widely. Furthermore some techniques require an auxiliary etchant gas such as NH_3 and H_2 commonly used in the synthesis of CNTs/CNFs. The dissociated carbon atoms are deposited through the surface of the catalyst particle on the substrate. Thus the smallest feature size of the CNF is governed by the catalyst shape and not from equipment precision as in the case of lithography methods.

C-CVD processes involve lower growth temperatures (400-1000 °C) and power inputs than laser ablation and arc discharge methods. Besides, the CNS do not need further purification and the technique can be scaled up to mass production.

2.3.4 Catalytic Plasma Enhanced Chemical Vapor Deposition

In a C-CVD process the involved gases are activated by the heat from the high processing temperature which makes it difficult to incorporate CNSs to CMOS technology whose circuits can usually withstand temperatures up to only 450 °C before being degraded. A possible solution to this problem is the use of alternative gas activation sources as in the case of the catalytic plasma enhanced chemical vapor deposition technique (C-PECVD) which uses the highly energetic electrons from a plasma to activate the dissociation process of the hydrocarbon gas source decreasing the required growth temperature.

According to the ways the plasma is generated different PECVD systems have been introduced such as alternating current (AC) PECVD, radio frequency (RF) PECVD, microwave PECVD and direct current (DC) PECVD.

The focus of this work is on VACNFs synthesis by DC plasma enhanced chemical vapor deposition (DC-PECVD). In this process the electric field during the growth assists in the fabrication of free-standing CNFs on top of solid substrates. The vertical alignment of the synthesized CNFs implies that the catalyst should remain at the tip of the fibers as stated before in this chapter. If the synthesis conditions during the DC-PECVD process are such that tip growth is initiated, the fibers will tend to follow the direction of the field. Thus, by adjusting either the position of the substrate with respect to the electric field or the geometry of the reactor, different alignments for the CNFs can be achieved. Figure 5 shows an example of VACNFs synthesized in our laboratory which are aligned according to the field direction. The crack on the sample seen at the bottom of the chip has changed the orientation of the substrate with respect to the electric field.

Because of the vertical alignment, controllable location and lower growth temperature provided by this deposition method the VACNF are attractive for NEMS applications. A detailed description of the DC-PECVD deposition method as well as the growth mechanisms of VACNFs is given in Chapter 3.

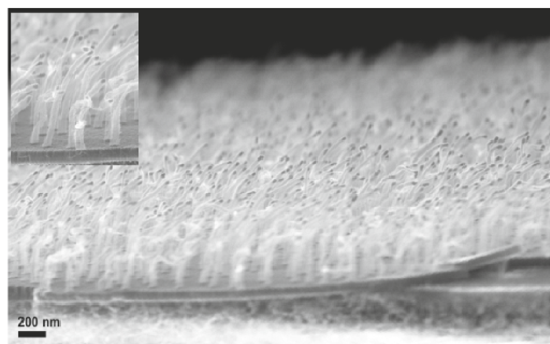

Figure 5- VACNFs vertical alignment is dictated by the direction of the electric field present during the PECVD synthesis.

3. DC-PECVD

In general a catalytic chemical vapor deposition process is based on the formation of a material on top of a substrate from the gas precursor dissociation aided by a catalyst in the interior of a vacuum chamber. The precursor molecules are vaporized and transported into the chamber. They diffuse, adsorb and decompose on the surface of the catalyst coated areas of the heated substrate. The functional molecules are incorporated into the solid material, and finally, the molecular by-products are recombined and released back into the gas phase.

In plasma enhanced catalytic chemical vapor deposition systems electrical energy is used to create a glow discharge (plasma) which promotes the creation of reactive radicals, neutrals, ions, electrons and other molecules from the gas mixture. These reactive species interact with the catalyst/substrate inducing either etching or deposition processes. Since all the highly energetic species are formed by collisions in the gas phase the substrate is exposed to a lower temperature in comparison to the thermal CVD process.

The main steps involved in the material deposition by means of a PECVD system shown in Figure 6 are

I) Glow discharge acceleration of ions and reactants towards substrate surface.
II) Surface reactions
III) Material deposition on the substrate surface
IV) Desorption of by-products from substrate

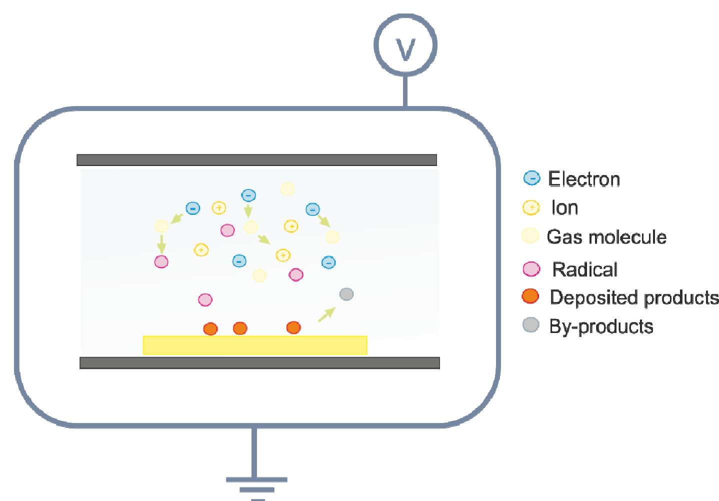

Figure 6. PECVD schematics

3.1 Plasma Sheath Distribution

Our system uses a DC plasma source to induce the chemical reactions cascade by applying an electric potential (100 V to several kV) between two conductive electrodes in a gas chamber. Once a certain voltage is achieved, a complex scheme of glow and non-glow regions is displayed between the electrodes as shown in Figure 7.

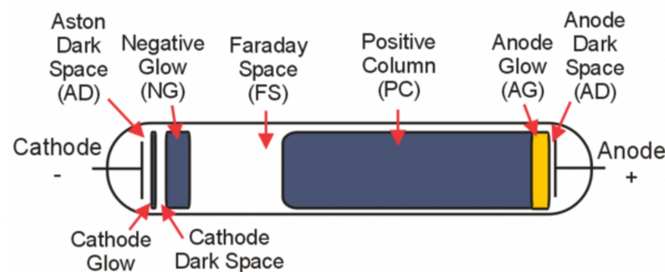

Figure 7. Schematics of glow discharge sheath distribution [24].

A glow discharge is a mixture of neutral atoms, electrons and ions. Since it has equal concentrations of positive and negative charges it is a neutral gas mixture. The plasma is sensitive to the presence of magnetic and electric fields so by applying an electric field between the two electrodes, free electrons are accelerated away from the cathode. When their kinetic energy is high enough collisions with neutral species make the latter to lose electrons, phenomenon known as ionization. The degree of ionization of the plasma will depend on the supplied energy to the system. The energy transfer of the system is governed by the electrons because of their mass being really low in comparison with the ions or the other heavier molecules present in the gas. Therefore, they will not lose energy to the plasma body. Other chemical processes apart from ionization also existing in the plasma are given in Table 1.

Inside the glow discharge, the gas zone known as the positive column or glow will be characterized by its high ionization and high temperature. This region owns its name to the visible radiation emission produced in the system from the energy and density of highly excited species the de-excitation of which produces emission of light. The ionization collisions generate electron-ion pairs. In the cathode dark space the positively charged ions will be accelerated towards the cathode, where they release secondary electrons which will be accelerated away from the cathode, in the negative glow space, giving as a result a self-sustained plasma.

Near to the area of the electrodes, the metallic vapors originating from vaporization processes mix with the gas phase inducing modifications to the local properties of the discharge. Their effect is to drain the extra current from the plasma in the anode glow area. Finally, dark spaces are created in which the excitation of the gas medium is too small that no light emission is observed.

The energy and the electric charge of the particles in the plasma change upon contact with solid surfaces. The highly energetic free electrons are able to break chemical bonds. They transfer energy to the surface making it active so that molecules in the material can be bound to molecules in the gas mixture, covering the surface with a specific material.

In contrast to CVD processes where the reactions are only thermodynamically possible at high temperatures, in the PECVD the deposition rate will depend on both the plasma density given by power and pressure and the reaction kinetics provided by temperature and plasma composition.

3.2 Plasma Chemistry

During the glow discharge the electrons accelerated away from the cathode will collide with other electrons, atoms or molecules in the gas chamber giving raise to different chemical reactions classified as electron collisions and atom- ion molecule collisions. Table 1 describes the reactions involved in a PECVD chamber.

Electron collisions		
Ionization	$e^- + A \rightarrow A^+ + 2e^-$	An ion is formed from the collision of a neutral particle with an electron with higher kinetic energy than the neutral ionization energy.
Recombination	$e^- + A^+ \rightarrow A$	An electron combines with a positive ion. The electric charge of the ion is neutralized due to the collision with a particle of opposite charge.
Electron attachment	$e^- + A \rightarrow A^-$ $e^- + AB \rightarrow AB^-$	This reaction allows the removal of electrons from electronegative gases. The electron attaches to the neutral molecule to create a negative ion.
Excitation	$e^- + A \rightarrow A^* + e^-$	A neutral species is changed to an excited state (A*) upon its collision with an electron which induces quantized transitions in the vibrational and rotational electron states
Dissociation	$e^- + AB \rightarrow A^* + B^* + e^-$	Molecules break apart into smaller fragments. These fragments, commonly named radicals, become highly chemically reactive enhancing and accelerating reactions.
Electron detachment	$A^- + B \rightarrow A + B + e^-$	Electron detachment is used to disintegrate negative atomic or molecular ions.
Dissociative attachment	$e^- + A_2 \rightarrow A^+ + A^- + e^-$	A neutral is split into individual ions by its collision with an electron.
Dissociative ionization	$e^- + AB \rightarrow A + B^+ + 2e^-$	An ion is created during the dissociation of a molecule.
Atom-ion molecule collisions		
Symmetrical charge transfer	$A + A^+ \rightarrow A^+ + A$	When ions collide with atoms of the either the same or a different type a charge transfer can occur.
Asymmetric charge transfer	$A + B^+ \rightarrow A^+ + B$	
Penning ionization	$A^* + AB \rightarrow AB^{+\cdot} + e^- + A$	Penning ionization occurs when an excited metastable atom/molecule reacts with a neutral molecule leaving it ionized. The products of the reaction are a radical molecular cation, an electron and a neutral gas molecule.

Table 1. Chemical reactions taking place in a PECVD system

3.3 Growth Mechanism of CNF

Several research studies have been performed in order to understand the growth mechanism of CNS, there are however still questions to be answered. Figure 8 describes the most accepted steps during CNS growth explained as follows:

1. Adsorption and decomposition of the hydrocarbon molecules on the catalyst surface.
2. Formation of carbon islands or film on the catalyst surface.
3. Diffusion of carbon species through the surface and/or the bulk of the catalyst and subsequent precipitation of carbon atoms to the opposite site of the catalyst favoring formation of graphene layers.
4. Continuos stacking of graphene layers to form the carbon filament.

In order to sustain the process it is important to keep active reaction sites on the catalyst surface available for more hydrocarbon dissociation. The carbon filament synthesis will stop when the kinetics of the system is such that a carbon film can poison the whole catalyst by blocking all possible reaction sites on its surface.

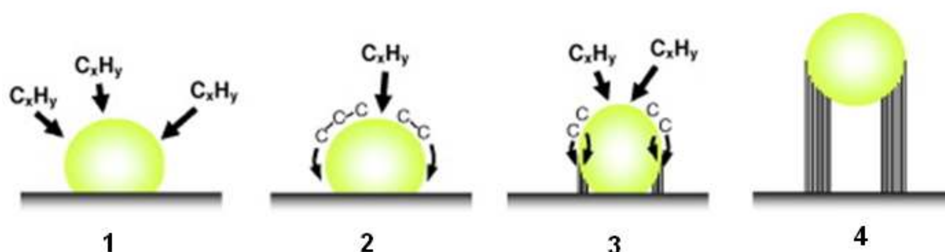

Figure 8. CNF growth mechanism[25].

There are different theories reported by several research groups, but there is still no consensus regarding the rate limiting step and the carbon diffusion path during the growth. Baker et al. suggested that the carbon diffuses through the metallic particle due to a temperature gradient, condensing carbon in the opposite site of the surface of the catalyst for the subsequent formation and precipitation of parallel planes of graphene[26]. They found an activation energy value comparable to that of the carbon diffusion in nickel suggesting carbon diffusion as the rate limiting step for the process. The catalytic growth suggests that the growth happens through the precipitation of carbon dissolved from the catalyst surface[27].

By changing the mixture of gases the growth rate of the CNS can be altered. Some research groups attribute it to the temperature gradient created from the catalytic reaction[22]. In contrast, Rotrup-Nielsen and Trim assume it is due to a concentration gradient[28]. Snoeck et al. proposed a mechanism of growth in which the carbon diffusion originates from a concentration gradient from the distinct solubility of carbon in the carbon-metal interface and in the metal itself[29]. Other research groups have proposed similar mechanisms[30,31].

Helveg et al. performed in situ TEM analysis verifying the crystallinity of the catalyst during growth and the formation of graphene layers on the step edges of a {111} surface of nickel[32].

3.4 Plasma Chemistry in the Synthesis of CNF/CNT from C_2H_2 and NH_3 precursors

In the synthesis of carbon nanostructures, acetylene (C_2H_2) and methane (CH_4) are commonly used as carbonaceous gases, while hydrogen (H_2) and ammonia (NH_3) are used as etchant gases to prevent amorphous carbon deposition which in turn poison the catalyst or degrade the CNF/CNT quality.

The plasma chemistry properties and conditions that lead to a deterministic CNF/CNT synthesis are not fully understood yet. However, some experimental and simulation studies [33,34,35] have provided a general insight of the dominant chemical reactions and chemical species in the plasma during growth. A brief summary of the most important findings for a mixture of NH_3/C_2H_2 growth precursors is presented in this section.

Plasma composition by mass spectroscopy (MS) and residual gas analysis (RGA) studies have been reported by the Milne and Meyyappan research groups[33,34]. By varying the C_2H_2 composition by changing the NH_3:C_2H_2 gas ratio, the main chemical reactions and species were reported. NH_3, C_2H_2, H_2, N_2 and HCN were detected as the main neutral species and NH_3^+, $C_2H_2^+$, HCN^+ NH_4^+, NH_2^+, and C_2H^+ as the main ions.

Acetylene has been suggested as the main source of carbon deposition during CNT/CNF formation since it has been found in plasmas that lead to CNT synthesis without being one of the feedstock gases[36] and other carbon carrying species (C_2, CH_4, etc.) have not been found in NH_3/C_2H_2 plasma studies[33]. In addition, Zhong et al. reported C_2H_2 as key precursor in the CVD synthesis method of SWCNTs[37].

Cruden et al.[34] have reported that certain hydrocarbon (methane) and hydronitrocarbon species (methylamine and methanimine) formed by methyl radical (CH_3) reactions display peak densities at the best deposition conditions of their experiment, thus suggesting CH_3 radicals as an important precursor in the growth of clean and well aligned carbon nanostructures in addition to acetylene.

Ammonia helps in the generation of hydrogen and hinders the decomposition of C_2H_2 by removal of carbon carrying species from the gas phase inhibiting their contact with the substrate/catalyst. For instance, HCN formed from the interaction of N with C_2H_2 has been found at high concentrations in highly ionized NH_3/C_2H_2 plasmas in which also a growth rate reduction was observed for CNT/CNFs[33]. The growth rate decrease can be explained by the lower decomposition of HCN than C_2H_2 at the catalyst surface due to their bond strength difference being 556 kJ/mol and 748 kJ/mol for HCN and C_2H_2 respectively[35].

NH_3 decomposition is preferred over C_2H_2 decomposition since the bonding strength in a NH_3 molecule is weaker than that of a C_2H_2 molecule. NH_3 and C_2H_2 dissociation increases with power and pressure[34].

Atomic hydrogen is responsible for the removal of excess carbon by combining and carrying away carbon atoms before their substrate deposition. Hydrogen is provided not only by ammonia but also by C_2H_2 dissociation as reported by the Milne research group[33]. High levels of hydrogen were observed at NH_3/C_2H_2 plasmas rich in either C_2H_2 or NH_3 and the minimum level of atomic hydrogen generation was at ~20% C_2H_2 composition[34].

An amorphous carbon deposition regime is usually observed at either high C_2H_2 composition or at high ionization levels supplied by plasma parameters (power, pressure, high electric fields, etc) which lead to the formation of subsidiary ions that can generate more carbon carrying species such as methylamine (CH_3NH_2), propiolonitrile (HC_3N), 1,3 butadiyne (C_4H_2) and propadiene (C_3H_4) exceeding the carbon that can be carried away from the etchant gas reactions[33,34] .

So far the results from plasma chemistry studies have provided a good understanding about the main active species present in the plasma near the substrate during CNF/CNT synthesis. However, a thorough catalyst surface reactions study is pending to draw clear conclusions about the chemical compounds and reactions taking place in the growth of CNS.

3.5 PECVD Reactor for Growth Study

The synthesis of the VACNFs is performed in the commercially available AIXTRON Black Magic PECVD reactor shown in Figure 9. It consists of a 2 inch wafer chamber and uses the cold wall system from integrated circuits deposition equipments. A graphite heater is used as both cathode and substrate holder. The substrate can be heated (maximum heater temperature 900 °C) by a fast response heater with ramp rates within 1 to 1000 °C/min. A thermocouple is embedded in the heater surface to allow independent control of the temperature in the substrate.

The gas precursors are mixed in the gas mixing system and then introduced into the chamber by a shower head acting also as the anode. The gas flow is directed towards the cathode. The showerhead

helps to uniformly distribute the gas flow along the substrate. A system of mass flow controllers (MFCs) is used to monitor the type and amount of the gases fed to the chamber.

The DC-glow discharge is generated by a DC plasma generator of 1 kW power with variable frequency (1-100 kHz). The maximum allowed current and voltage are 2.5 A and 800 V respectively. The voltage, current and power parameters are coupled as in the majority of dc glow discharge reactors which is a serious drawback of this deposition system. A mechanical pump provides an operating pressure of 1-10 mBar.

Figure 9. AIXTRON black magic PECVD reactor.

4. VACNF Catalyst Patterning and Growth Sequence

As has been mentioned in Chapter 1, the objective of this work is the optimization of VACNFs synthesis for their future use as NEMS building blocks. This chapter explains in detail the fabrication processes involved in the pre-patterning of catalyst on the substrate and the standard growth conditions for the synthesis of the VACNFs.

In general, the process is depicted as follows: a TiN underlayer is sputtered onto the substrate to act as a diffusion barrier for silicide formation. Colloidal lithography is used to create the pattern for the catalyst on the substrate. Then nickel is evaporated on the pre-patterned susbstrate to obtain nickel catalyst dots and finally, the AIXTRON Black Magic II PECVD reactor is employed to synthesize the VACNFs.

4.1 Substrate Preparation

A 3 inch silicon wafer with 400 nm thick thermally grown SiO_2 is used as a carrier. The substrate is cleaned with isopropyl alcohol (IPA- C_3H_8O) and blow dried with an N_2 gas stream.

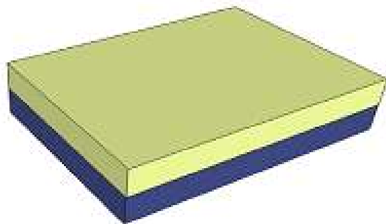

A 100 nm TiN film is deposited with a dc magnetron sputtering system called FHR-MS150. The parameters of the deposition are: base pressure < 3 x 10^{-6} mbar, flow rates of 92 sccm Ar and 3 sccm N_2, deposition pressure of 5 x 10^{-3} mbar, a current of 1.9 A and a power of 460 W.

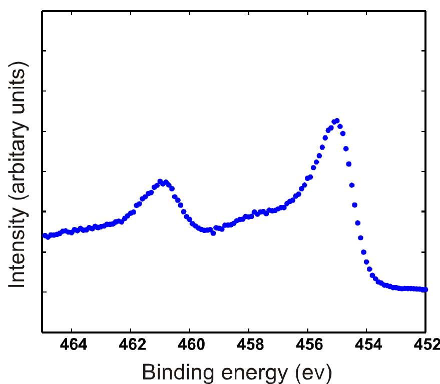

X-ray photoelectron spectroscopy (XPS) and resistivity measurements were used to characterize the stoichiometry of the sputtered TiN film. Figure 10 shows the XPS spectrum of the Ti 2p level of the TiN film; the peaks at 455 eV and 461 eV verify the presence of the TiN bonds. The resistivity value of 37 μΩ cm, obtained from the sheet resistance value measured by a four point probe set up and the thickness of the film measured by a surface profiler, is in agreement with previously reported data [46,47,48] . Please refer to appendix A for more details about the reproducibility and characterization of the TiN film.

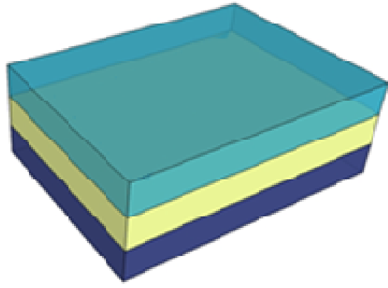

A resist layer is spun onto the substrate to act as a sacrificial layer. The resist is MCC950K PMMA A4. The spinning velocity is 4000 rpm with an acceleration of 3000 rpm for 1 min to obtain a 200 nm thickness. Then a soft bake process of 5 min at 170 °C is performed. Finally, the substrate is exposed to a 5 sec O_2 plasma treatment at 50 W, 250 mTorr and 10 sccm flow to improve the substrate surface hydrophilicity and promote a uniform distribution of solutions in the next deposition steps (Fredriksson et al. 2007) .

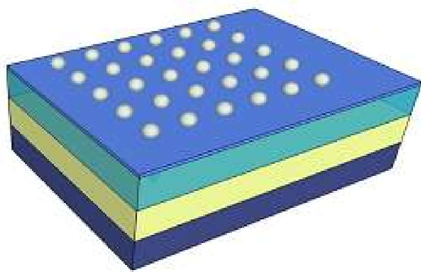

The cationic poly(diallyldimethylammonium) electrolyte (PDDA) is pipetted onto the PMMA layer for 45 s and is then rinsed with running DI water and blow dried with N_2 to generate a positively charged surface. The negatively charged solution of polystyrene nanoparticles (sulfate latex 80 ± 20 nm) is pipetted onto the PDDA surface for 3 min to achieve saturation coverage. After this follow rinsing with running DI water (10 s), immersion in boiling water (40 s) and blow drying with N_2. The purpose of the boiling water immersion is to prevent particle 2D/3D aggregations by increasing the contact adhesion of the adsorbed particles to the surface.

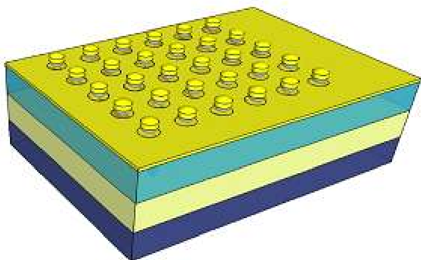

A 10 nm Au film is e-beam evaporated (AVAC HVC 600 equipment) on the nanoparticle-covered surface. The deposition parameters are: base pressure $3x10^{-6}$ mbar, I=40 mA and deposition rate 1 Å/s. It is worth noting that the deposition angle controls the geometry of the mask holes. In our case, the deposition was done normal to the substrate so we expect to reproduce the circular projection of the deposited nanoparticle spheres.

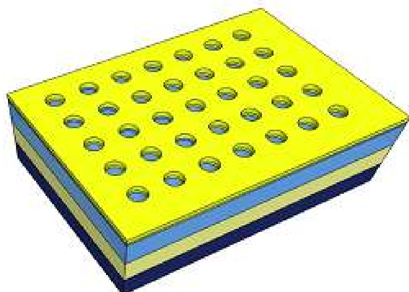

The nanoparticles are removed from the substrate surface by carefully adhering and then stripping an adhesive tape (STW-10 tape).

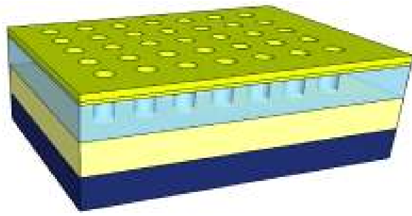

The substrate is then plasma etched with a flow of 10 sccm O_2 during 5 min to remove the PMMA underneath the holes and transfer the pattern of the mask. The etching parameters are: a power of 50 W and 250 mTorr of pressure.

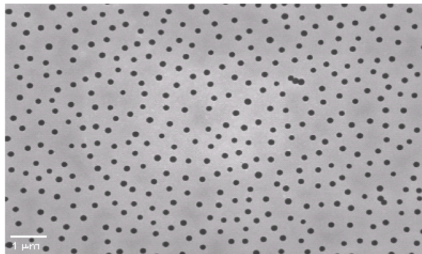

The SEM micrograph in Figure 11 shows the result of the hole mask colloidal lithography on the Si/SiO_2/TiN substrates. The holes have a diameter of 80 ± 20 nm showing a successful transfer of the nanoparticle´s shape and distribution.

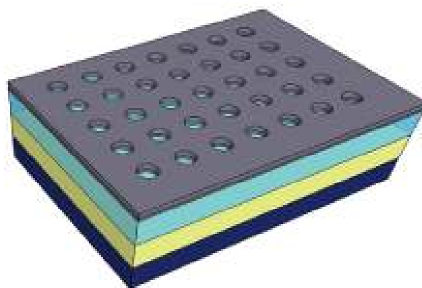

After the substrate has been lithographically patterned a layer of Ni catalyst is e-beam evaporated (AVAC HVC 600) onto the substrate. The evaporation process parameters are: base pressure ≤ 3.0 x10^{-6} mBar, I=70-80 mA (adjusted by deposition rate), deposition rate=2 Å/s yielding a final thickness of 50 nm.

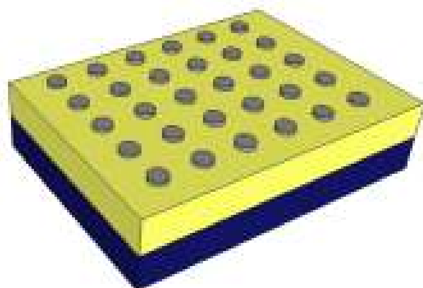

The catalyst pattern is transfer to the Si/SiO2/TiN by lifting it off in 1165 remover at 70 °C for a time ≥ 15 min, then the substrate is immersed in IPA for a time ≥ 10 min for a subsequent cleaning by a quick dump rinse (QDR) process cycle. Finally, the substrate is blow dried with N_2.

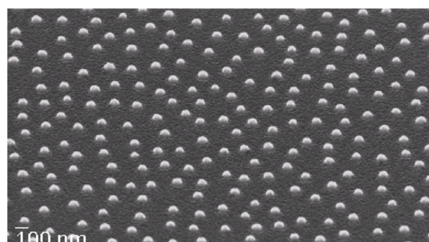

Figure 12 shows a SEM micrograph of the resulting Ni catalyst seeds on top of the TiN diffusion barrier. It can be seen that hole colloidal lithography method can be used to control the distribution and shape of the catalyst seeds.

4.2 Growth Sequence

There are three main steps in the synthesis of VACNFs: annealing of the sample by heating the substrate holder to the desired temperature (usually between 500 ˚C and 700 ˚C); a plasma pre-treatment of several seconds to help in the dewetting of the catalyst, the reduction of the surface oxide on the catalyst and the plasma stabilization before the carbon source is provided and finally; the introduction of the carbon source gas to the plasma which will initiate the fiber growth.

The growth sequence for the VACNFs synthesis into the PECVD chamber is as follows:

1. The substrate is placed in the substrate-holder (cathode) at room temperature.
2. The chamber is closed and pumped to a pressure of 0.2 mBar.
3. NH_3 is introduced in the chamber at a flow of 160 sccm and a pressure of 4 mBar to heat the substrate to the desired annealing temperature (600-700 °C) at a selected ramp rate (100-300 °C/min).
4. A plasma treatment ranging from 15 to 30 sec is performed in an NH_3 ambient at the desired growth flow (120-480 sccm) and power (40-200 W). The plasma power is controlled by setting the voltage to 800 V and limiting the current to 500 mA.
5. The growth is initiated by introducing the carbonaceous gas source (C_2H_2) in the chamber at the required flow rate (30-120 sccm). Unless the flow rate is a parameter of study a carbon to etchant gas ratio of 1:4 is normally used during the growth sequence.
6. The heater is set to the desired growth temperature (600-800 °C) at the required ramp rate.
7. The growth phase is usually maintained during 15 min.
8. The plasma, heater and gases are turned off.
9. The system is cooled down to a temperature $T \leq 50$ °C while still in vacuum.
10. The sample is removed from the substrate holder and the chamber is pumped down again to maintain the vacuum condition.

It is worth mentioning that the optimization growth study was performed by altering one or several parameters during the growth sequence. If the parameter change during the growth study (Chapter 4) is not mentioned the following standard conditions prevail:

Pretreatment (annealing) step:	Temperature: 600 °C
	Ramp rate: 300 °C/min
	Gas environment: NH_3 (160 sccm)
Plasma treatment:	Time: 15 sec
	Gas environment: NH_3 (120 sccm)

	Power: 80 W
Growth step:	Time: 15 min
	Carbon to etchant gas ratio: 1:4
	Power: 80 W

To verify the growth results a scanning electron microscope (SEM Zeiss Supra 60VP) and a transmission electron microscope (TEM JEOL JEM2100) were used.

The SEM is equipped with a CCD camera with IR illumination. The system was operated with an acceleration voltage of 20 kV and tilting angles of 40-60° were used for image acquisition.

The samples for TEM were prepared by cutting the chip in several sharp wedge pieces subsequently mounted in silver wires using conductive epoxy glue and then placed in the sample holder. The e-beam, operated at 100 keV, was incident parallel to the Ti-N surface of the samples. The images were taken with a digital camera (Gatan SC1000).

The reproducibility of the PECVD synthesis of VACNFs relies on the control of a large parameter space. The chemical reactions present in the PECVD CNFs synthesis are governed by the type and the density of the neutral and charged species present during the growth process. Controlling the rate and the desired chemical reactions is not a trivial task especially when several factors can affect the final outcome. For instance, changes in the PECVD system parameters (e.g. pressure, temperature, gas flow rate, etc.) result in different chemical environments leading to differences in the as-grown VACNFs.

Even though a repeatable tuning of the parameters such as pressure, gas flow rates, power, etc. has been achieved for our PECVD system we have found it challenging to control the actual temperature the chip is exposed to during the growth of the fibers. The PID module and thermocouple used to provide and monitor the temperature of the heater during the growth were effectively controlled but temperature gradients across the heater and between the heater and the substrate have been found to be significant when comparing resulting VACNFs from subsequent growths at same growth conditions. Nonetheless, the trends observed in the PECVD parameters growth study were validated with several growth trials and can be considered as reproducible.

Reproducibility of the colloidal lithography and the reactive sputtering process for TiN have been validated (results not shown) in previous studies performed at our laboratory. Effects of variations coming from the catalyst and substrate were minimized given that all the samples used for a given experiment were always fabricated in the same lot.

5. Results

In this chapter the results from the growth study will be explained. The optimization of the VACNFs synthesis was determined from all the following results: the effect of each growth parameter in the synthesis of the VACNFs, the influence of the fabrication steps on the quality of the as-deposited fibers and the proposed growth model based on a study of the initial growth phase.

5.1 Annealing Treatment

The growth of VACNF is done at considerably high temperatures; therefore it is necessary to evaluate the thermal stability of the as-deposited TiN diffusion barrier. The film should prevent silicide formation and enhance the catalyst nucleation for the growth. Three different annealing temperatures with a 100 °C/min ramp rate were evaluated (600, 650, 700 °C) using substrates with a Ni thickness of 50 nm. The results are shown in Figure 13.

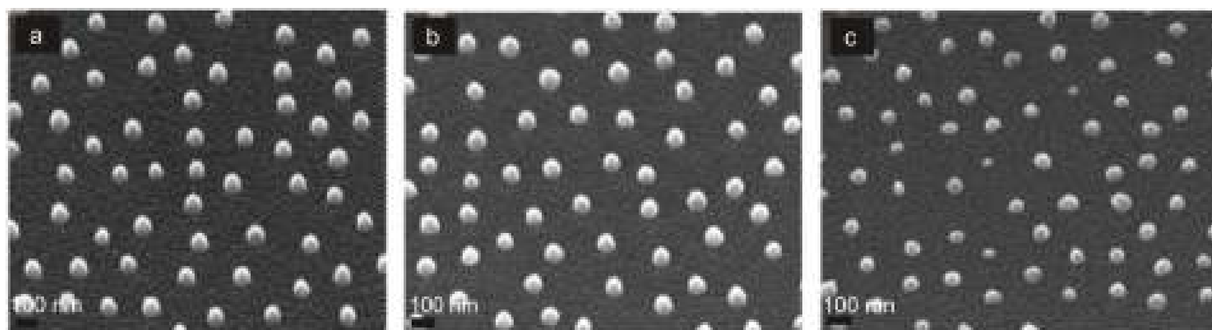

Figure 13. Ni catalyst nucleation after exposure to annealing treatments at a) 600 ˚C, b) 650 ˚C and c) 700 ˚C with a 100 ˚C/min ramp rate and NH_3 ambient (160 sccm).

The catalyst particles show uniform diameters and have become spherical during the heat treatment at 600 and 650 °C. However, when the samples were annealed at 700 °C, diffusion of Ni into the TiN film is noticeable and caused the particles' sphericity and uniformity to decrease.

These observations can be explained by the fact that at high temperatures the TiN performance as a diffusion barrier is affected by the microscopic defects (e.g. grain boundaries, voids, etc.) in its structure so that the catalyst particles can interact with the underlying barrier material, forming

dislocations and/or precipitations by means of diffusion. Nowak, W. B. et al. reported an increase in Ni weight fraction versus time at several annealing temperatures for TiN films[38].

We have reported that discrepancies in the stoichiometry of reactively sputtered TiN films increase the resistivity and decrease the failure temperature of the barrier in a previous work (please refer to appendix A for more details). Our findings are in agreement with Park, K. C. and Kim, K. B. who also studied the importance of the density and microstructure on TiN films performance as a diffusion barrier[39] .

Based on the previous observations and on the final aim of using the VACNFs for NEMS it has been decided to proceed with an annealing treatment at 600 °C with a ramp rate of 300 °C/min which assures a successful nucleation of catalyst particles without diffusion into the TiN underlayer.

5.2 Plasma Pretreatment

The effect of plasma treatment during the transition between annealing and growth process in the VACNF synthesis was assessed by exposing the samples to different lapses (30, 60 and 90 sec) of NH_3 plasma after an annealing treatment at 600 °C with a ramp rate of 300 °C/min. Results are shown in Figure 14.

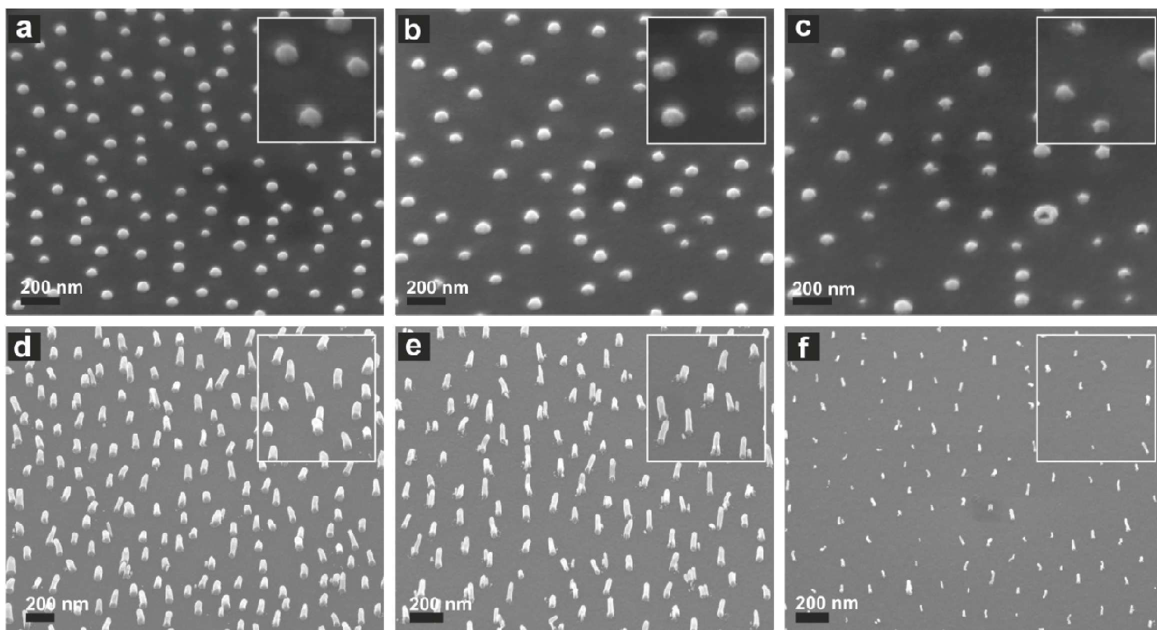

Figure 14. Ni catalyst seeds upon exposure to annealing process and NH_3 plasma treatment at 40 W during a) 30 s, b) 60 s and c) 90 s. VACNFs were synthesized with a 600 ˚C annealing process and NH_3 plasma treatment at 120W during d) 15s, e) 60 s, f) 300 s. NH_3 plasma treatment defines the degree of etching on the catalyst before the growth is started.

As the plasma exposure time increased the nucleated catalyst particles diffusion and surface area etching pits were noticed even more due to a roughing of the TiN/Ni surface and the etching effects of the NH_3 plasma ions. Ren Z. F., et al. reported the use of ammonia plasma exposure for the thinning down of nickel catalyst films for VACNT synthesis[40] .

Since the exposure on the samples under ammonia plasma even at the lowest interval of 30 sec showed the effect of etching, as reflected in the Figure 14 insets, it is necessary to make a transition from annealing to growth process as fast as possible to avoid side effects on the nucleated catalyst particles without compromising both the cleaning of the substrate surface from oxides and the stability of the plasma before growth is started. A plasma treatment of 15 sec was utilized in every growth unless something else is specified.

This trend was verified also during a complete VACNFs deposition. Figure 14d-f shows the results. As expected the density of the fibers decreased as the plasma exposure was increased from d) 15s to e) 1 min and finally to f) 5 min. At the longest plasma treatment we can barely see growth since the catalyst has been etched significantly. The growth was made at 600 °C, 120 W and 30/120 (C_2H_2/NH_3) and it lasted only 2 min after each plasma treatment.

5.3 Oxygen Plasma Treatment on TiN

Intermediate processing steps from catalyst deposition to carbon nanofiber synthesis could influence the quality of the synthetized VACNFs. We adopted colloidal lithography for Ni catalyst patterning. An inherent step of this process is the exposure of the sample to oxygen plasma ashing which in turn oxidizes the TiN film. The presence of an oxide layer on the surface could affect the synthesis of the fibers. During the annealing phase O_2 could interact with Ni and/or TiN varying the nucleation of the catalyst. To verify this idea, a growth trial at 80 W, 60:240 (C_2H_2/NH_3), 6.45 mBar was done during 15 min on three samples. These samples were reactively sputtered with 100 nm TiN and then coated with a 15 nm Ni film. Two of them were exposed to an oxygen plasma treatment at different durations one to 10 s and the other to 60 s before the catalyst deposition. Differences in density and diameter distributions over the substrates were encountered for different durations as shown in Figure 15 suggesting that an oxide layer on the TiN barrier modifies the catalyst dewetting during the annealing process. The lack of knowledge about the repeatability of this phenomenon given that it was done only one time impedes the formulation of a clear explanation about the differences seen in the catalyst dewetting among the samples.

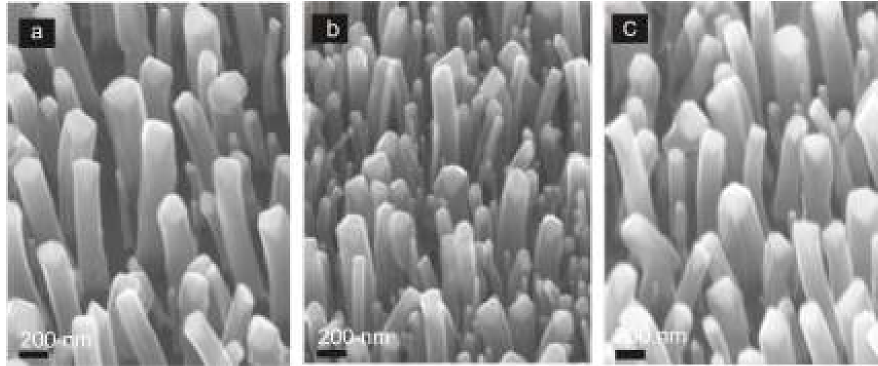

Figure 15. VANCFs synthesized from 15 nm Ni films on top of a) TiN film without O_2 plasma treatment b) TiN film exposed to an O_2 plasma of 50 W during 10 s and c) TiN film exposed to O_2 plasma of 50 W during 60 s.

These observations highlight the importance of considering the pre-processing steps and their effect on the surface of the catalyst and the substrate for the growth. For instance, by having in mind the idea of making NEMS devices with the VACNFs, other lithographic techniques such as e-beam lithography could be needed which not necessarily will required an oxygen plasma ashing before the catalyst deposition. If this is the case, compensation for this fact should be considered when defining the optimum conditions for the synthesis of the fibers.

5.4 Effects of Growth Parameters

5.4.1 Growth Temperature

The minimum growth temperature should be high enough to activate the catalytic activity on the metal particle surface which enables growth. The decomposition of hydrocarbons commonly used for CNF/CNT synthesis occurs at temperatures of 500 °C or more[15]. We synthesized VACNFs within the range of 550 °C to 750 °C. By increasing the growth temperature we increased the growth rate of the VACNFs as shown in Figure 16 where the length of the resulting fibers change from 390 nm to 570 nm by a thermal increase of 50 °C while keeping other parameters constant.

The diffusion of carbon on the catalyst surface is temperature dependant, thus an increase in carbon supply from the catalyst surface to graphene nucleation sites accelerate the carbon filament formation. We have reported activation energy of 0.3 eV for our system. This value is comparable with previous values of 0.23 eV and 0.5 eV reported in previous studies[41,42] and suggests carbon diffusion as the main limiting step in the growth in our chamber.

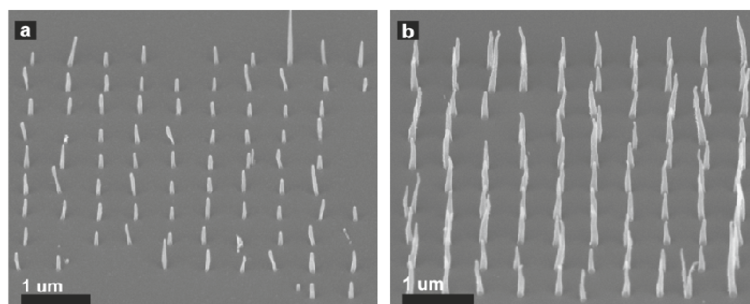

Figure 16. VACNF synthesized at 600 ˚C (300 ˚C/min ramp rate) annealing, 100 W, 50:100 sccm C_2H_2:NH_3 and growth temperature of left: 600 ˚C and right: 650 ˚C during 15 min. An increase in growth rate is seen as result of growth temperature increase.

5.4.3 Gas Pressure

In contrast to previously reported results[43] the VACNFs growth rate decreases with an increase in total pressure in our system as shown in Figure 17a-d. The pressure was increased from 3.32 mBar to 4.61 mBar then to 6.65 mBar and finally to 9.29 mBar. This was done by varying the gas flow rates in the PECVD chamber.

By increasing the pressure in the system a higher level of ionization is expected in the plasma which in turn will lead to a higher amount of collisions among the particles present in the ionized gas. At the same time, a higher ionization will increase the electric field in the plasma sheath enhancing the vertical alignment of the CNF. The relative amount of carbon bearing species will be higher in the plasma and the reactive nucleation sites of the catalyst surface will be gradually reduced slowing down the hydrocarbon decomposition process which at extreme cases could poison the catalyst and stop the growth as mentioned in Chapter 3.

At too high pressures (Figure 17d) a transition to the base growth mode in the case of our TiN/Ni substrate was found. Further explanation about this fact will be addressed under the growth mechanism section of this Chapter.

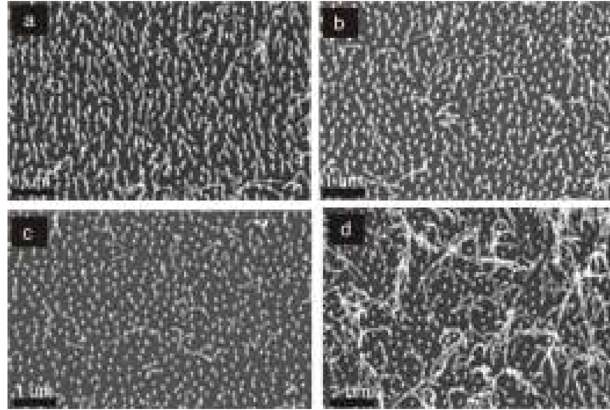

Figure 17. VACNF synthesized at 600 ˚C (300 ˚C/min ramp rate) annealing, 120 W, 600 ˚C and a) 3.32 mBar, b) 4.61 mBar, c) 6.65 mBar and d) 9.29 mBar for 2 min. A decrease in the growth rate and a transition to mainly base type fibers is seen after increasing chamber pressure during the growth.

5.4.4 Gas Ratio

To study the influence of gas ratio we increase the concentration of acetylene while keeping everything else constant. As shown in the Figure 18 a-c the best deposition conditions are within 20 and 30% C_2H_2 since lower concentrations results in thin and defective carbon nanofibers while higher concentrations give rise to amorphous carbon deposition at the sidewalls causing the fibers to look more pyramid like.

At low concentrations of acetylene, NH_3 etching is the dominant process giving rise to defects along the structure of the fiber. As the C_2H_2 concentration is increased a higher carbonaceous source in the plasma compensates for the etching, stabilizing the deposition of graphitic carbon and the removal of amorphous carbon. However, when the C_2H_2 concentration is too high the relative amount of NH_3 in the plasma is reduced; the deposition of carbon is much higher than the etching rate giving rise to amorphous carbon deposition along the fiber sidewalls as seen in Figure 18c.

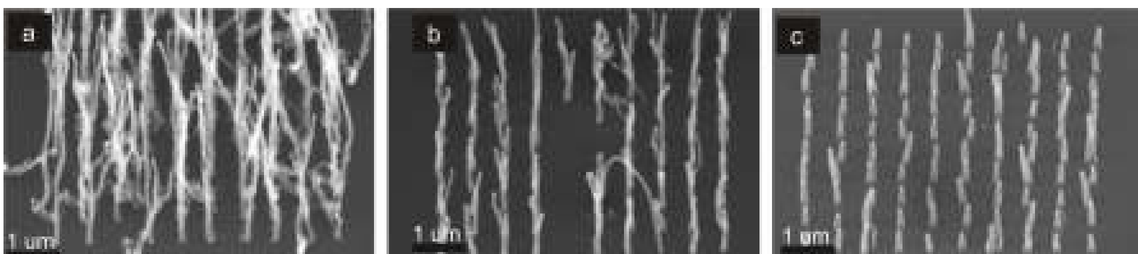

Figure 18. VACNFs after 10 min growth at 120 W, 6.45 mBar and a) 10% C_2H_2 b) 20% C_2H_2 and c) 33% C_2H_2.

5.4.5 Power

In DC-PECVD systems the plasma voltage and current are coupled, limiting the possibility to control each of these factors separately. An increase in power in this system results in both higher voltage and higher current which strengthens the plasma electric field as well as the degree of ionization. As seen in Figure 19 an increase in growth rate was found as the power was varied from 40 W to 150 W. The quality of the fibers seems to degrade at high powers because of the high level of decomposition of the feedstock gases which change the dominant plasma species in each case leading to different deposition characteristics. For instance, higher NH_3 decomposition at high powers will provide more H and will remove carbon bearing species from the plasma enhancing the etching effect as seen for 100 W and 150 W in Figure 19.

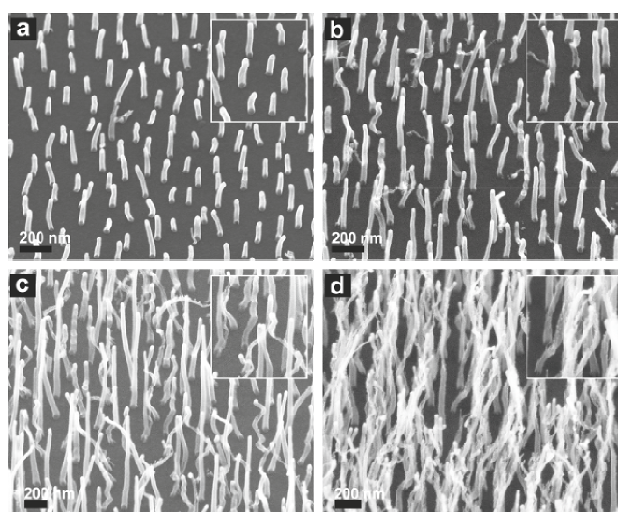

Figure 19. VACNFs after 15 min growth at a) 40W, b) 70W, c) 100 W and d) 150 W. The insets in the images correspond to a 300X magnification. Etching effects (seen by the CNF body degradation) increases as power increases.

5.5 Growth Repeatability

In order to illustrate the degree of repeatability of our system two sequential growth trials under the same growth conditions are shown in Figure 20. The quality of the VACNFs is not at the optimum growth conditions. The growth parameters are neither in the optimum range nor constant over the growth time. These kinetic variations during the growth have caused a continuous change in the plasma chemistry as well as in the catalyst structure perhaps these being the main reasons for the twisting appearance of some of the fibers.

Discrepancies in the appearance and distributions of the length and thickness of the fibers can be noticed from Figure 20a-d. During the growth study, we realized that the system is highly sensitive to local variations in temperature. Even though the control of the temperature is repeatable from the PECVD system perspective, the transfer of the heat from the heater to the substrate is mainly done through radiation which could be affected by the heater conditions. Irregularities in the graphite heater such as aging or the impurities coming from carbon deposits from previous growths can alter the effective transfer of the heat to the substrate.

Future synthesis where the placement of the substrate is fixed and the heater is routinely changed and/or cleaned could probably improve the reproducibility of the resulting VACNFs.

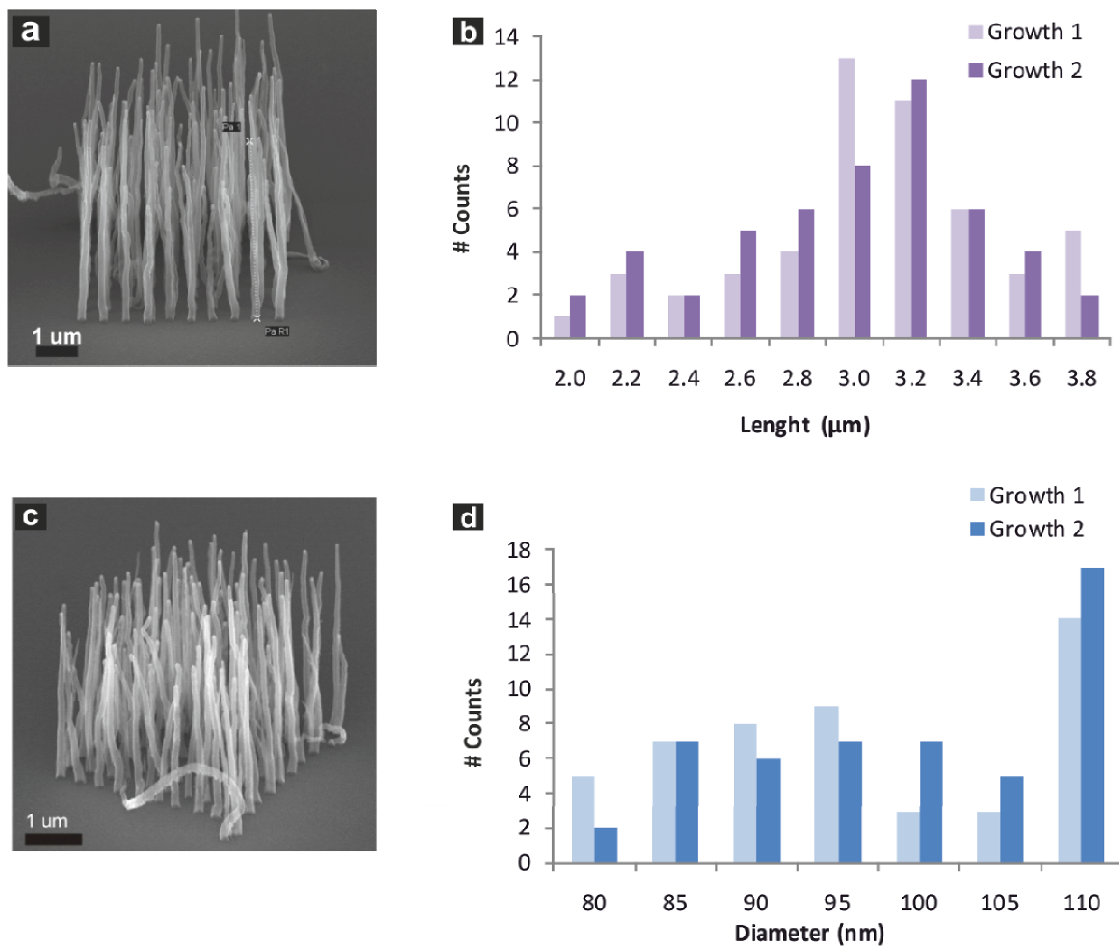

Figure 20. VACNF growth repeatability. 2 trials of the same growth recipe are shown a-c). The growth parameters were: 600˚C (300˚C/min), 120W, 600˚C during 2.5 min and then 700˚C, 180W during 10 min. b-d) histograms of the length and diameter for both trials were obtained from a series of SEM images; perspective corrections were taken into account with an angle of 60°.

5.6 Growth Mechanism

On the way to optimize the growth of the vertically aligned carbon nanofibers continuous transitions between curly unaligned nanofibers and well aligned VACNFs were observed. It has been demonstrated by Merkulov et al. that the presence of the catalytic particle at the tip of the CNF is crucial for its vertical alignment. Anyhow, we confirmed the presence of the catalyst at the bottom and at the tip of the nanofibers as seen in Figure 21.

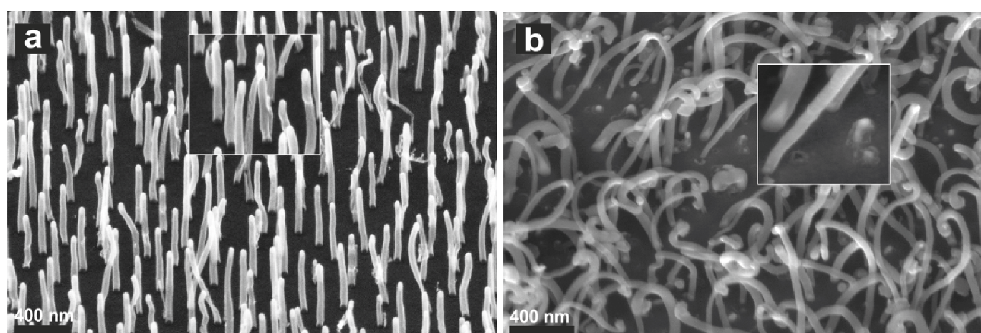

Figure 21. Carbon nanofibers synthesized in Black Magic PECVD reactor during the growth study. a) Vertically aligned carbon nanofibers having tip growth mode were obtained as seen from the catalyst remaining at the tip of the fiber body. b) Unaligned carbon nanofibers (base growth mode) having the catalyst particle trapped at the bottom of the fiber can be observed.

Previous studies on the subject have been reported. Song et al.[44] have proposed the adhesion force between the substrate and the catalyst as the main factor defining the growth mode of the fibers. They claim that a strong adhesion force will anchor the catalyst to the substrate leading to a base type growth. In their turn, Gohier et al. [25] reported correlations between the catalyst particle size and the growth mode. None of these arguments can help to fully explain the observations from our set-up. All of the samples used in our experiments are made out of the same materials deposited under the same conditions. Special attention has been put in using samples from the same batch to perform each parameter study. On the other hand, we have seen transitions from base to tip growth at both small and large thickness of catalyst. Melechko et al.[45]suggested that growth mode transitions can be obtained by changing the growth parameters and that for each parameter a critical value can be defined which denote the limit between transitions.

From these observations and reported data it can be deduced that the initial phase of the growth, in which nucleation sites for posterior carbon diffusion are defined, is the main step controlling the growth mode of the synthesized carbon nanostructures. On this basis, whatever is the preferred

growth mode at the beginning of the synthesis, this will be preserved even though the growth conditions are further changed in favor of the opposite growth mode during the synthesis process.

In order to sustain this line of research a multistep growth was performed where the initial conditions of growth were chosen to favor tip growth and subsequent steps previously known for yielding base type fibers were applied. The results, shown in Figure 22, confirm the existence of VACNFs as expected from the first growth step.

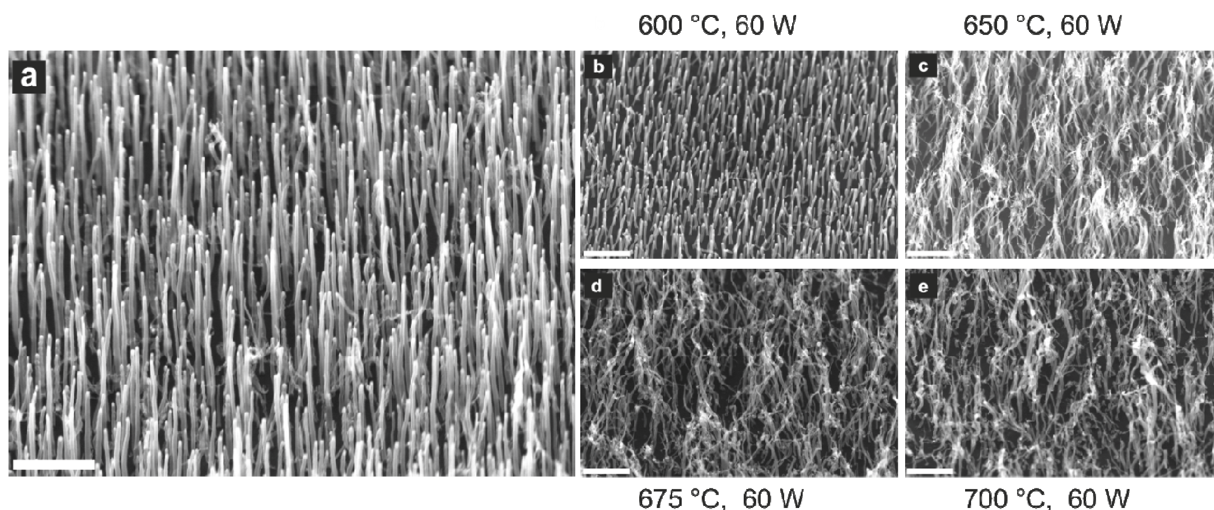

Figure22. a) Multistep synthesis. Annealing temperature of 600 ˚C (300 ˚C/min), 15 s plasma pretreatment, gas ratio was set to 30/120 sccm (C_2H_2/NH_3), plasma power of 60 W and temperature increments from 600 ˚C to 650 ˚C and to 700 ˚C every 2 min. b-d) Single step synthesis showing the resulting fibers from each step applied separately. All chips have a 50 nm thick Ni catalyst.

The next step was to investigate the initial phase of the growth to get a better understanding of the mechanism behind these transitions. One of the first observations during SEM sample analysis was the characteristic shape of all the catalysts, shown in Figure 23, which resembles a crystal structure. This finding has been reported before by Helveg et al.[32]. Furthermore, an analysis of the structure of the VACNFs under TEM revealed that the fibers' catalysts expose {111} planes to the plasma environment during the growth (please refer to Figure 23b-c). Hong et al. reported that different facets in the nickel crystal show different carbon solubilities. Facets (111) and (110) have activation energy for carbon diffusion of 0.4 eV while (100) facets are far less reactive with activation energy of 2.1 eV. The activation energy of our process (0.3 eV) is in agreement to the TEM results since (111) facets have a small energy barrier therefore promoting carbon diffusion for the formation of the graphite sheets along the [110] plane direction. From this information we can conclude that our system agrees with the sequential growth model explained in Chapter 3 having diffusion of carbon as main rate limiting step.

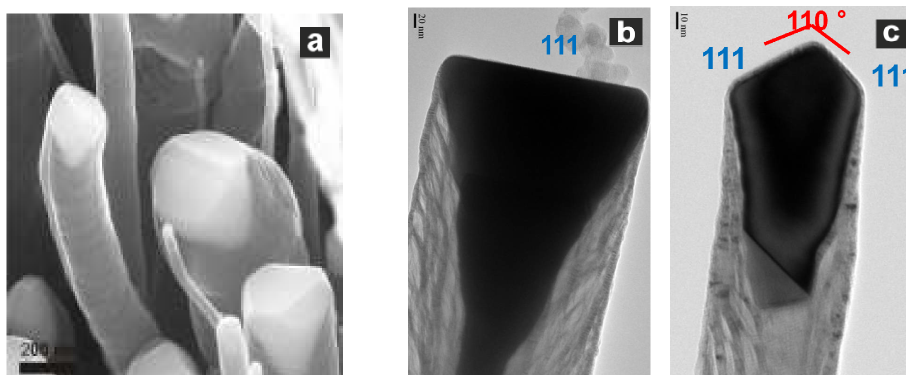

Figure 23. a) A typical shape of the catalyst present at the tip of the VACNFs seen under SEM. The shape resembles a crystal with different facets. b-c) TEM images of the VACNFs showing { 1 1 1 } planes exposed to the plasma. The fiber is oriented along [1 1 0] direction.

The results from the initial phase growth study for the VACNFs have been presented in detail elsewhere (please refer to appended paper A) and are in agreement with the previously reported trends in the parameter study discussed in previous sections of this chapter. The growth rate increased as a result of higher temperature and power. In contrast, the growth rate decreased by increasing the plasma pressure of the system. This can be explained by a shift of the growth to a supply-limited state either by the arrival or the decomposition of the carbon bearing species on the catalyst surface. The dominant chemical species present in the plasma for synthesis with C_2H_2 and NH_3 gas sources have been discussed in Chapter 3. HCN and C_2H_2 are the main chemical species in the ionized gas and C_2H_2 is reported as the main precursor for the growth. Therefore, the increase in pressure induced an increase in the carbon bearing species, shifting the system in favor of acetylene formation. In addition, the amount of atomic H is not sufficient to maintain the surface of the catalyst free of carbon deposits reducing the amount of active sites for diffusion of C which in turn decreases the growth rate.

Similarly, the transition between the two growth modes can be explained in terms of the ability of the system to maintain the catalyst active diffusion facets free of carbon deposits at the initial phase of the growth. If the system is unbalanced in favor of acetylene formation, a competition between the formations of the first graphene sheets on the catalyst surface or the catalyst/substrate interface will exist. When the latter prevails, meaning the catalyst surface was covered with carbon deposits to a large extent, the catalyst is anchored to the substrate and base type carbon nanofibers are synthesized.

The formation of such carbon deposits are narrowly related to both the geometry of the catalyst and its crystallographic orientation after nucleation. For instance, if the catalyst exposes the carbon diffusion reactive facets to the plasma at the beginning of the growth an anchorage of the catalyst will be less likely to happen than if the less reactive facets are exposed since the energy barrier to be

overcome will be higher. Besides, if the more reactive facets are facing the substrate that will imply a carbon diffusion path from the substrate/catalyst interface to the catalyst surface since the fiber most likely will be still aligned along the reactive [110] direction.

Further studies on the diffraction pattern of the base type fibers could lead to a better conclusion on the growth transitions and the higher deposition rate as compared with the tip type growth.

5.6 VACNF Growth Optimization

After having a better understanding of both the growth mechanism and the effect of each growth parameter in the synthesis of the fibers, an optimization process can be carried out.

In order to obtain good alignment we need to control the electric field strength in the plasma by means of power. The power should be high enough to provide good ionization but not too high to avoid the etching effects on the sidewalls of the CNF as previously observed. A good interval of power has been found to be 40-90 W.

It is worth to mention again that base type growth usually leads to irregular unaligned CNF growth and can be avoided by the choice of catalyst and substrate materials as well as growth conditions; the selection of the growth parameters should subsequently be done in accordance with the required final results.

In our case tip growth mode fibers are of interest. Therefore, a growth temperature of 550-600 °C was used and when necessary the temperature was increased after the growth was started to avoid transitions to base growth seen at higher temperatures. The growth temperature is related to the degree of graphitization of the CNF (crystallinity). In addition, at growth temperatures higher than 700 °C a competition of higher carbon diffusion rate versus lower sticking coefficient of carbon to the catalyst surface is present giving as result a decrease in the growth rate[15].

The gas ratio was tuned between 20% and 26% of acetylene concentration to provide enough carbon for deposition and yet keep enough NH_3 in the plasma to remove the amorphous carbon. The gas pressure was tuned together with the gas flow where pressures between 4 mBar and 6.9 mBar were used for the synthesis. Figure 24 shows an example of a synthesis with parameters within the range of optimization.

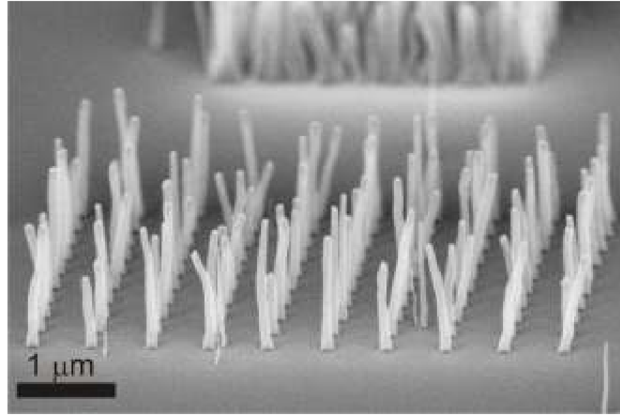

Figure 24. An example of good VACNF growth on top of TiN. The growth was performed at 600 ˚C (300˚ C/min) during 5 min, 80 W and 21.3% C_2H_2.

The growth rate has been proven to be constant over time as shown in Figure 25 where the length of the VACNFs increase from 1 µm to 2 µm as a result of an increase in growth time from 15 to 30 min. A fine tuning of the length of the CNFs can be achieved by only modifying the growth time since the quality of the fibers is not affected by time.

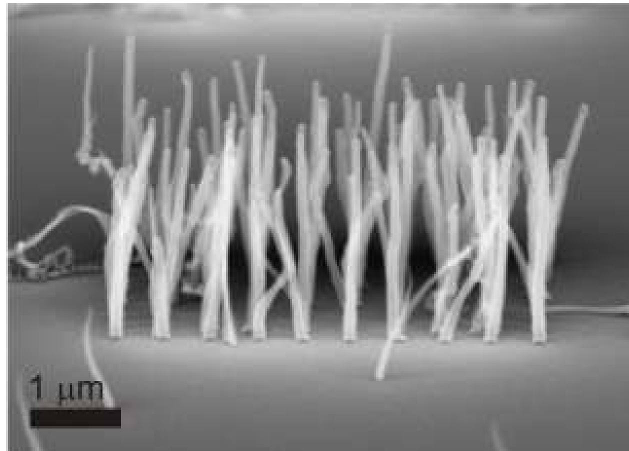

Figure 25. VACNFs growth after 30 min. The growth was performed at 600 ˚C (300 ˚C/min) during 5 min, 80 W and 21.3% C_2H_2. CNFs quality was preserved over time.

6. Conclusions

The feasibility of using TiN film as a diffusion barrier for the synthesis of vertically aligned carbon nanofibers has been demonstrated. It prevents the diffusion of Ni into the Si/SiO_2 substrate during the annealing process and can be deposited in a repeatable and reliable manner.

Optimal growth conditions for the synthesis of vertically aligned carbon nanofibers were defined for the Black Magic II PECVD system after performing a growth parameter study.

The initial growth phase was analyzed in detail providing a new insight of the mechanism behind the synthesis of the carbon nanostructures. It has been suggested that when there is a balance between the carbon formation and the etching, by means of hydrogenation, a diffusion limited process is observed. When the system instead is slanted in favor of carbon formation, carbon deposits on the surface of the catalyst reduces the amount of reactive sites for carbon diffusion giving as a result a supply limited growth mechanism.

Analogously, the transitions between aligned tip type and nonaligned base type carbon nanofibers are explained in terms of the orientation of the first graphitic planes formed either at the catalyst surface or at the catalyst/substrate interface.

Further studies on the structure of the base type fibers by TEM could provide with valuable information about the crystallographic orientation of the catalyst. This information can not only provide an explanation for the differences in the carbon diffusion paths which lead to misaligned fibers but also elucidate the principle behind the higher growth rate observed in this type of fibers.

The control over the synthesis of the VACNFs is a complex task. The failure to reproduce identical fibers with maintained growth conditions suggests that it may be difficult to eliminate all the variations in the system. Therefore, the optimum growth conditions for the VACNFs should be defined in terms of their intended use. It can be said, from experience, that there is not an ideal growth recipe to synthetize carbon nanofibers. However, by having a good understanding of the growth mechanism and the effect of each parameter in the synthesis reactor, functional VACNFs can be obtained by compensating any undesired effect which deviate the system from an equilibrium between carbon deposition and the hydrogen etching of amorphous carbon from the catalyst surface during the growth.

Acknowledgments

I would like to thank my supervisors Farzan Alavian Ghavanini and Per Lundgren for their support and encouragement in exploring my research interests. They gave me the confidence to try any new idea and the necessary guidance from the beginning to the end of this project.

I am thankful for the wonderful time I had with all the members of the Bionano Systems Lab who make of this journey an enriching and fun experience.

7. References

1. Waser, R. Nanoelectronics and Information Technology-Advanced Electronic Materials and Novel Devices. (2005).

2. Thostenson, E. Advances in the science and technology of carbon nanotubes and their composites: A review. *Composites Science and Technology* **61**, 1899-1912 (2001).

3. Mao, Z., Garg, A. and Sinnott, S.B. Molecular dynamics simulations of the filling and decorating of carbon nanotubules. *Nanotechnology* **10**, 273-277 (1999).

4. Poncharal, P., Wang, Z.L., Ugarte, D. and De Heer, W.A. Electrostatic Deflections and Electromechanical Resonances of Carbon Nanotubes. *Science* **283**, 1513-1516 (1999).

5. Kim, P. and Lieber, C.M. Nanotube nanotweezers. *Science* **286**, 2148-2150 (1999).

6. Rinkiö, M., Johansson, A., Paraoanu, G.S. and Törmä, P. High-speed memory from carbon nanotube field-effect transistors with high-kappa gate dielectric. *Nano Letters* **9**, 643-647 (2009).

7. Isacsson, A., Kinaret, J.M. and Kaunisto, R. Nonlinear resonance in a three-terminal carbon nanotube resonator. 16 (2006).at <http://arxiv.org/abs/cond-mat/0612589>

8. Jin, H. et al. Detection of single-molecule H2O2 signalling from epidermal growth factor receptor using fluorescent single-walled carbon nanotubes. *Nature Nanotechnology* **5**, 302-309 (2010).

9. Kaul, A.B., Wong, E.W., Epp, L. and Hunt, B.D. Electromechanical carbon nanotube switches for high-frequency applications. *Nano Letters* **6**, 942-947 (2006).

10. Cid Salavert, C.C. Sensors based on carbon nanotube field effect transistors and molecular recognition approaches. 209 (2008).doi:ISBN:978-84-692-1533-3

11. Dresselhaus, M.S., Dresselhaus, G. and Jorio, A. Unusual Properties and Structure of Carbon Nanotubes. *Annual Review of Materials Research* **34**, 247-278 (2004).

12. "Reprinted with permission from Melechko, A.V. et al. Control of carbon nanostructure: From nanofiber toward nanotube and back. *Journal of Applied Physics* **102**, 074314 copyright (2007), American Institute of Physics."

13. Züttel, A. Hydrogen storage in carbon nanostructures. *International Journal of Hydrogen Energy* **27**, 203-212 (2002).

14. Merkulov, V.I., Melechko, A.V., Guillorn, M.A., Lowndes, D.H. and Simpson, M.L. Alignment mechanism of carbon nanofibers produced by plasma-enhanced chemical-vapor deposition. *Applied Physics Letters* **79**, 2970 (2001).

15. Melechko, A V. et al. Vertically aligned carbon nanofibers and related structures: Controlled synthesis and directed assembly. *Journal of Applied Physics* **97**, 041301 (2005).

16. Zhou, C., Kong, J. and Dai, H. Intrinsic electrical properties of individual single-walled carbon nanotubes with small band gaps. *Physical Review Letters* **84**, 5604-5607 (2000).

17. Zhang, L. et al. Four-probe charge transport measurements on individual vertically aligned carbon nanofibers. *Applied Physics Letters* **84**, 3972 (2004).

18. Cassell, A.M., Austin, A.J., Krishnan, S., Meyyappan, M. and Yang, C.Y. Characteristics of aligned carbon nanofibers for interconnect via applications. *IEEE Electron Device Letters* **27**, 221-224 (2006).

19. Ruoff, R.S., Qian, D. and Liu, W.K. Mechanical properties of carbon nanotubes: theoretical predictions and experimental measurements. *Comptes Rendus Physique* **4**, 993-1008 (2003).

20. Callister, W.D. and Wiley, J. MATERIALS SCIENCE AND ENGINEERING Sixth Edition. *Materials Science* 101 (2003).

21. McCreery R L. Carbon Electrodes: structural effects on electron transfer kinetics. *Electroanalytical Chemistry, A.J. Bard (Ed), Dekker, NY* **17**, 221-374 (1991).

22. Baker, R.T.K., Thomas, R.B. and Waite, R.J. Formation of Filamentous Carbon from Iron , Cobalt and Chromium Catalyzed of Acetylene Decomposition. *Atomic Energy* **95**, 86-95 (1973).

23. Iijima, S. Helical microtubules of graphitic carbon. *Nature* **354**, 56-58 (1991).

24. Reprinted with permission from Creative commons directive. http://creativecommons.org/licenses/by/2.5/deed.en. Electric glow discharge. (2008).at <http://www.plasma-universe.com/Electric_glow_discharge?title=Electric_glow_discharge&printable=yes>

25. "Reprinted from Carbon, 16, Gohier, A., Ewels, C., Minea, T. and Djouadi, M, Carbon nanotube growth mechanism switches from tip- to base-growth with decreasing catalyst particle size, 1331-1338 Copyright (2008), with permission from Elsevier"

26. Baker, R.T.K., Barber, M.A., Harris, P.S., Feates, F.S. and Waite, R.J. Nucleation and growth of carbon deposits from the nickel catalyzed decomposition of acetylene. *Journal of Catalysis* **26**, 51-62 (1972).

27. Oberlin, A., Endo, M. and Koyama, T. Filamentous growth of carbon through benzene decomposition. *Journal of Crystal Growth* **32**, 335-349 (1976).

28. Trim, R.-N.J. and N. *Catalyst* **48**, 155 (1977).

29. Snoeck, J.W., Froment, G.F. and Fowles, M. Filamentous Carbon Formation and Gasification: Thermodynamics, Driving Force, Nucleation, and Steady-State Growth. *Journal of Catalysis* **169**, 240-249 (1997).

30. Alstrup, I. A new model explaining carbon filament growth on nickel, iron, and Niz.sbnd;Cu alloy catalysts. *Journal of Catalysis* **109**, 241-251 (1988).

31. Pinheiro, J.P. and Gadelle, P. Chemical state of a supported iron-cobalt catalyst during CO disproportionation I. Thermodynamic study. *Journal of Physics and Chemistry of Solids* **62**, 1015-1021 (2001).

32. Helveg, S. Atomic-scale imaging of carbon nanofiber growth. *Nature* **427**, 426-429 (2004).

33. Bell, M.S. et al. Plasma composition during plasma-enhanced chemical vapor deposition of carbon nanotubes. *Applied Physics Letters* **85**, 1137 (2004).

34. Cruden, B.A., Cassell, A.M., Hash, D.B. and Meyyappan, M. Residual gas analysis of a dc plasma for carbon nanofiber growth. *Journal of Applied Physics* **96**, 5284 (2004).

35. Hash, D.B. et al. An investigation of plasma chemistry for dc plasma enhanced chemical vapour deposition of carbon nanotubes and nanofibres. *Nanotechnology* **16**, 925-930 (2005).

36. Woo, Y. In situ diagnosis of chemical species for the growth of carbon nanotubes in microwave plasma-enhanced chemical vapor deposition. *Diamond and Related Materials* **11**, 59-66 (2002).

37. Zhong, G. et al. Acetylene: A Key Growth Precursor for Single-Walled Carbon Nanotube Forests. *The Journal of Physical Chemistry C* **113**, 17321-17325 (2009).

38. Nowak, W.B. Diffusion of nickel through titanium nitride films. *Journal of Vacuum Science Technology A Vacuum Surfaces and Films* **3**, 2242 (1985).

39. Park, K.-C., Kim, K.-B., Raaijmakers, I.J.M.M. and Ngan, K. The effect of density and microstructure on the performance of TiN barrier films in Cu metallization. *Journal of Applied Physics* **80**, 5674 (1996).

40. Ren, Z.F. Synthesis of Large Arrays of Well-Aligned Carbon Nanotubes on Glass. *Science* **282**, 1105-1107 (1998).

41. Chhowalla, M. et al. Growth process conditions of vertically aligned carbon nanotubes using plasma enhanced chemical vapor deposition. *Journal of Applied Physics* **90**, 5308 (2001).

42. Hofmann, S. Low-temperature plasma enhanced chemical vapour deposition of carbon nanotubes. *Diamond and Related Materials* **13**, 1171-1176 (2004).

43. Bell, M.S. et al. Carbon nanotubes by plasma-enhanced chemical vapor deposition. *Pure and Applied Chemistry* **78**, 1117-1125 (2006).

44. Song, I.K., Cho, Y.S., Choi, G.S., Park, J.B. and Kim, D.J. The growth mode change in carbon nanotube synthesis in plasma-enhanced chemical vapor deposition. *Diamond and Related Materials* **13**, 1210-1213 (2004).

45. Melechko, A. Transition between "base" and "tip" carbon nanofiber growth modes. *Chemical Physics Letters* **356**, 527-533 (2002).

46. Fleischer, M. Geochemistry by□?. Prentice-Hall, Inc., NJ: 1979, xii 498 pp., . *Organic Geochemistry* **1**, 183 (1979).

47. Sundgren, J., Johansson, B., Karlsson, S. and Hentzell, H. Mechanisms of reactive sputtering of titanium nitride and titanium carbide II: Morphology and structure2. *Thin Solid Films* **105**, 367-384 (1983).

48. Schiller, S., Beister, G. and Sieber, W. Reactive high rate DC sputtering: Deposition rate, stoichiometry and features of TiOx and TiNx films with respect to the target mode. *Thin Solid Films* **111**, 259–268 (1984).

49. Fredriksson, H. et al. Hole–Mask Colloidal Lithography. *Advanced Materials* **19**, 4297-4302 (2007).

PAPER I

Growth characterization of vertically aligned carbon nanofibers on top of TiN buffer layer for nanoelectromechanical devices.

F. Alavian Ghavanini, M. Damian, D. Rafieian, P. Lundgren.

Procedia Engineering, 24th Eurosensors Conference Linz, Austria, Sep 05-08, 2010. 5 s. 1115-1118**.**

ELSEVIER

Available online at www.sciencedirect.com
ScienceDirect

Procedia Engineering 5 (2010) 1115–1118

Procedia Engineering

www.elsevier.com/locate/procedia

Proc. Eurosensors XXIV, September 5-8, 2010, Linz, Austria

Growth characterization of vertically aligned carbon nanofibers on top of TiN buffer layer for nanoelectromechanical devices

Farzan A. Ghavanini*, Maria E. L. Damian, Damon Rafieian, and Per Lundgren

Microtechnology and Nanoscience departement, Chalmers University of Technology, 41296 Göteborg, Sweden

Abstract

Initial growth of vertically aligned carbon nanofibers (VACNFs) from Ni catalyst seeds in the range of 40 to 100 nm as fabricated using hole-mask colloidal lithography on top of reactively sputtered TiN is studied. We observe that the initial growth conditions could cause a growth mode transition from base-type to tip-type. We attribute this transition to a change in the crystallographic orientation of the Ni catalyst seeds induced by initial growth conditions. A convenient method to deposit stoichiometric TiN films is also presented.

© 2010 Published by Elsevier Ltd.

Keywords:Vertucally aligned carbon nanofiber; VACNF; Titanium Nitride; Plasma enhanced CVD; Growth.

1. Introduction

The synthesis of vertically aligned carbon nanofibers (VACNFs) using catalytic plasma enhanced chemical vapor deposition (c-PECVD) in which position, diameter, length, and alignment of the nanofibers are accurately determined has offered an unprecedented opportunity to realize new nanoelectromechanical systems (NEMS) [1, 2]. The performance of such devices is crucially dependent on the electrical properties of the underlying electrodes. However, excellent candidates for the electrodes material such as copper and gold are not known to yield successful VACNF synthesis. A possible solution to incorporate these materials is to deposit a thin buffer layer between them and the catalyst seeds. Being known as an effective diffusion barrier [3], titanium nitride has been nominated for this purpose because of its VACNF synthesis compatibility [4] as well as its CMOS compatibility [5] which is an important parameter for future NEMS integration. In this paper we demonstrate a method to conveniently deposit stoichiometric TiN films. We adopt the hole-mask colloidal lithography to inexpensively study the growth of carbon nanofibers from patterned Ni catalyst seeds in the range of 40 to 100 nm. We pay a special attention to the transition of the growth mode from non-aligned base-type to well-aligned tip-type on top of the TiN substrates. Understanding and controlling this transition is of great importance when VACNF-based device fabrication is in mind.

1877-7058 © 2010 Published by Elsevier Ltd.
doi:10.1016/j.proeng.2010.09.306

2. Experimental

TiN films were deposited by reactive sputtering on top of thermally oxidized silicon with an oxide thickness of 400 nm using a commercial dc magnetron sputtering system (FHR-MS150) with a base pressure of less than $3 \circ 10^{-6}$ mbar. The system was equipped with an optical spectrometer which monitored the emission spectrum from the glow discharge during the deposition. The deposition was performed at flow rates of 92 sccm and 3 sccm of argon and nitrogen, respectively. The deposition pressure was $5.0 \circ 10^{-3}$ mbar. To produce stoichiometric TiN films we changed the magnetron current and monitored the plasma response from the optical spectrometer while the flow rates of both gases were kept constant. This method of sputtering TiN films offers more stability and reproducibility compared with the traditional method of changing the N_2 partial pressure [6]. The sheet resistance of the deposited film was measured in a four-point-probe setup within 2 minutes after the chips were exposed to the atmosphere in order to control the level of the film oxidation. The film resistivity was then calculated by taking into account the thickness of the deposited film as measured by a surface profiler (Tencor P15). We adopted hole-mask colloidal lithography [7] to conveniently produce Ni catalyst seeds in a diameter range of 40 to 100 nm on top of the TiN films. Three groups of chips with different thicknesses of Ni seeds (15, 30, and 50 nm) were deposited in an electron-beam evaporation chamber.

The annealing of the catalyst seeds and the VACNF synthesis were performed in an AIXTRON Black Magic PECVD reactor. In the annealing step the chips were heated from room temperature to 600 °C (300 °C per minute) in an ammonia atmosphere at 4 mbar. The annealing step was followed by a 15 s ammonia plasma treatment at the target plasma power. The growth step was followed immediately by introducing acetylene into the chamber. The C_2H_2/NH_3 flow ratio was fixed at 0.25 in all the growth trials. The grown nanofibers were then studied using scanning electron microscopy (SEM).

3. Discussions

Figure 2.A shows the typical behavior of a reactive sputtering system indicating a drastic decrease in the intensity of the Ti peak as read from the optical spectrometer at a certain magnetron current. Although the gas flow rates are kept constant, a change in the magnetron current modifies the rate at which nitrogen is incorporated into the target. This translates into a change in the nitrogen partial pressure in the chamber when a TiN layer is formed on the target surface which can be detected from the plasma optical emission. It should be noted that the formation of the TiN layer on the target occurs at different points for increasing and decreasing magnetron currents as explained by the Berg model [8, 9] giving rise to the hysteresis observed in Figure 1.a. The optimum magnetron current for the deposition of a stoichiometric TiN is the lower current value in the transition region [6] of Figure 1.A (1.9 A). The optimum deposition point results in the minimum film resistivity as depicted in Figure 1.b.

In order to optimize the quality of the VACNFs on top of the TiN substrates we paid a special attention to the initial growth phase as it is significantly influenced by the substrate [10]. For this purpose, synthesis of VACNFs was carried out for 2 minutes and was abruptly terminated by turning off the plasma and the substrate heater. Figure

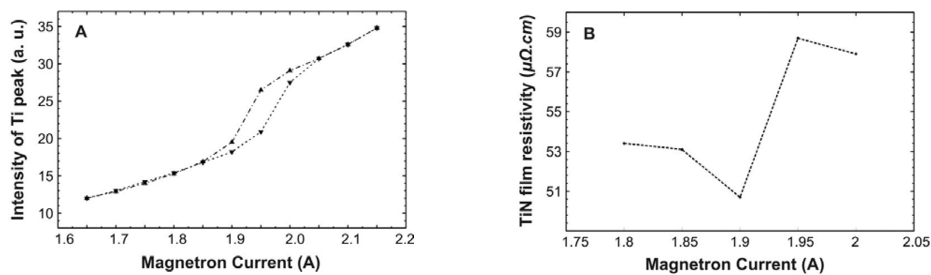

Fig. 1. (a) The intensity of the Ti peak as read from the optical spectrometer as a function of the magnetron current. (▲) shows the decreasing and (▼) shows the increasing current path; (b) The resistivity of the TiN as measured versus the magnetron current.

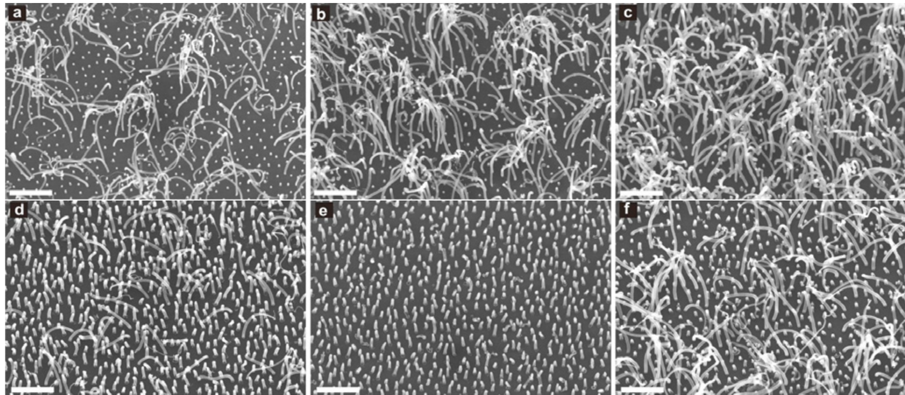

Fig. 2. (a-c) Synthesis of Ni seeds with different thickness (a) 15 nm, (b) 30 nm, and (c) 50 nm on top of TiN substrates at 600 °C and 4 mbar, C_2H_2/NH_3 gas ratio of 30/120sccm, and plasma power of 60W. (d-f) synthesis of 50 nm thick Ni seeds on top of TiN substrates at 600 °C, plasma power of 120W, and C_2H_2/NH_3 gas ratio and pressure of (c) 15/60 and 2 mbar, (d) 30/120 and 4 mbar, (e) 150/600 and 10 mbar

2.a to 2.c shows the effect of the catalyst thickness on the growth of VACNFs. We observe that the population of base-type fibers increases as the thickness increases. This is in contrast with the explanation proposed by Song *et al.* [11] who argued that the growth mode is governed by the adhesion force between the catalyst and the substrate since the catalysts are deposited on identical substrates. Figure 2.d to 2.f shows a transition from base to tip mode and then going back to base mode by increasing the gas flow rates (and therefore the pressure) while keeping all the other growth parameters fixed. This observation cannot be explained by the formation of a carbon cap on the catalyst which prohibits the tip-type growth as proposed by Melechko *et al.* [12] because increasing the acetylene content while keeping the plasma power constant results in an increased carbon deposition [12] and therefore the base-type growth should be promoted.

In order to explain these observations we propose a new mechanism governed by the nucleation of the catalyst seeds before the growth initiates. It has been reported that the Ni particles are crystalline during the growth scenario [13]. Moreover, it has been concluded that different facets of a crystalline Ni nanoparticle show different reactivity to the carbon precursor gas [14] as well as different diffusion coefficients for carbon atoms [15]. Therefore we suggest that if during the annealing step the more reactive (100) and (110) surfaces of Ni are exposed to the plasma a tip growth mode is initiated while if these surfaces are attached to the substrate and less reactive (111) surface is exposed then a base growth mode is observed. The factors that determine the final exposed facets include the annealing and the growth conditions as well as the initial conditions of the Ni seed such as its thickness and

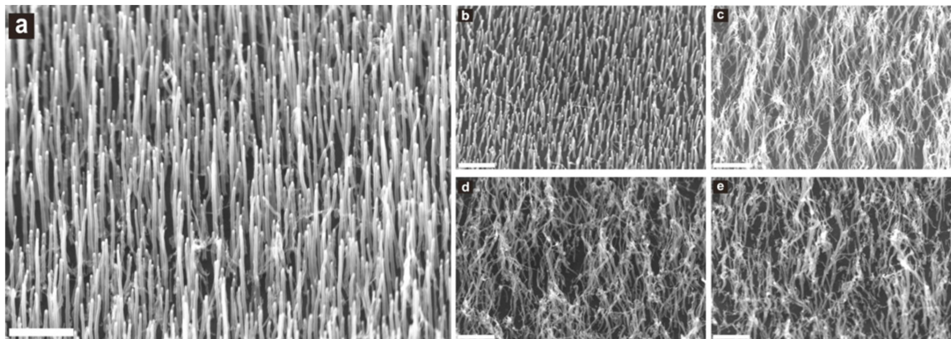

Fig. 3. (a) Four-step synthesis on 50 nm thick Ni seeds. The gas ratio of 30/120 sccm (C_2H_2/NH_3) and plasma power of 50 W was fixed during the entire process but the temperature was set to 600°C, 650°C, 675°C , and 700°C at each step. Each step last for 2 minutes. (b-c) Shows the resulting nanofibers on identical catalyst/substrate system when each step is applied separately on four chips.

diameter. In addition, the interaction with the substrate is an important factor that modifies the crystallographic orientation of the exposed facets [16]. To support our claim, we performed a multi-step growth including four steps beginning with growth conditions that are known to yield tip-type VACNFs while each of the next three steps result in base-type nanofibers if applied directly after the annealing step (see Figure 3.b to 3.e). The result shows (see Figure 3.a) well aligned VACNFs as expected from only the first growth step. This emphasizes that when a set of conditions that exposes the right Ni facets is applied and the growth is initiated, the consequent steps will not change the growth mode nor inhibit the tip growth.

4. Conclusions

We presented a convenient method to reproducibly deposit stoichiometric TiN films using reactive sputtering. The quality of the deposited film was examined from its resistivity. We also presented an inexpensive method to deposit Ni seeds in a diameter range of 40 to 100 nm using hole-mask colloidal lithography in order to study the growth of VACNFs from patterned catalyst seeds. We paid a special attention to the initial growth phase of the nanofibers and proposed that the growth mode of the carbon nanofibers depend on the crystallographic orientation of the Ni surfaces exposed to the plasma. This suggestion was supported by a multi-step growth process in which growth conditions known for yielding base-type nanofibers was performed after an initial growth step promoting tip-type VACNFs. The results showed that when a tip-type growth mode is initiated the consequent steps will not alter the growth mode nor inhibit the tip growth.

References

[1] Jang, J.E., et al.; Nanoelectromechanical switches with vertically aligned carbon nanotubes. Applied Physics Letters, 2005. 87(16): p. 163114-1.

[2] Jang, J.E., et al.; Nanoscale memory cell based on a nanoelectromechanical switched capacitor. Nature Nanotechnology, 2008. 3(1): p. 26-30.

[3] Garcia-Cespedes, J., et al.; Optimal deposition conditions of TiN barrier layers for the growth of vertically aligned carbon nanotubes onto metallic substrates. Journal of Physics D-Applied Physics, 2009. 42(10).

[4] Teo, K.B.K., et al.; Field emission from dense, sparse, and patterned arrays of carbon nanofibers. Applied Physics Letters, 2002. 80(11): p. 2011-2013.

[5] Wittmer, M. and H. Melchior; Applications of TiN thin-films in silicon device technology. Thin Solid Films, 1982. 93(3-4): p. 397-405.

[6] Berg, S., T. Larsson, and H.O. Blom; The Use of Nitrogen Flow as a Deposition Rate Control in Reactive Sputtering. Journal of Vacuum Science & Technology a-Vacuum Surfaces and Films, 1986. 4(3): p. 594-597.

[7] Fredriksson, H., et al.; Hole-mask colloidal lithography. Advanced Materials, 2007. 19(23): p. 4297.

[8] Berg, S., et al.; Modeling of reactive sputtering of compound materials. Journal of Vacuum Science & Technology A (Vacuum, Surfaces, and Films), 1987. 5(2): p. 202-7.

[9] Berg, S., et al.; Predicting thin-film stoichiometry in reactive sputtering. Journal of Applied Physics, 1988. 63(3): p. 887-91.

[10] Melechko, A.V., et al.; Vertically aligned carbon nanofibers and related structures: Controlled synthesis and directed assembly. Journal of Applied Physics, 2005. 97(4): p. 39.

[11] Song, I.K., et al.; The growth mode change in carbon nanotube synthesis in plasma-enhanced chemical vapor deposition. Diamond and Related Materials, 2004. 13(4-8): p. 1210-1213.

[12] Melechko, A.V., et al.; Transition between 'base' and 'tip' carbon nanofiber growth modes. Chemical Physics Letters, 2002. 356(5-6): p. 527-33.

[13] Helveg, S., et al.; Atomic-scale imaging of carbon nanofibre growth. Nature, 2004. 427(6973): p. 426-429.

[14] Schouten, F.C., O.L.J. Gijzeman, and G.A. Bootsma; INTERACTION OF METHANE WITH NI(111) AND NI(100) - DIFFUSION OF CARBON INTO NICKEL THROUGH THE (100) SURFACE - AES-LEED STUDY. Surface Science, 1979. 87(1): p. 1-12.

[15] Hong, S.L., Y.H. Shin, and J. Ihm; Crystal shape of a nickel particle related to carbon nanotube growth. Japanese Journal of Applied Physics Part 1-Regular Papers Short Notes & Review Papers, 2002. 41(10): p. 6142-6144.

[16] Baker, R.T.K.; Catalytic Growth of Carbon Filaments. Carbon, 1989. 27(3): p. 315-323.

PAPER II

Controlling the initial phase of PECVD growth of vertically aligned carbon nanofibers on TiN.

F. Alavian Ghavanini, M. Lopez-Damian, D. Rafieian, K. Svensson, P. Lundgren and P. Enoksson (in press).

Sensors and Actuators A: Phys, 2011,doi:10.1016/j.sna.2011.04.036

G Model
SNA-7366; No. of Pages 12

ARTICLE IN PRESS

Sensors and Actuators A xxx (2011) xxx–xxx

Contents lists available at ScienceDirect

Sensors and Actuators A: Physical

journal homepage: www.elsevier.com/locate/sna

Controlling the initial phase of PECVD growth of vertically aligned carbon nanofibers on TiN

Farzan A. Ghavanini [a,*], Maria Lopez-Damian [a], Damon Rafieian [a], Krister Svensson [b], Per Lundgren [a], Peter Enoksson [a]

[a] *Micro and Nanosystems Group, Department of Microtechnology and Nanoscience (MC2), Chalmers University of Technology, Göteborg, Sweden*
[b] *Department of Physics and Electrical Engineering, Karlstad University, SE-651 88 Karlstad, Sweden*

A R T I C L E I N F O

Article history:
Available online xxx

Keywords:
Vertically aligned carbon nanofiber
VACNF
TiN
PECVD synthesis
Growth mechanism

A B S T R A C T

We explore the growth of vertically aligned carbon nanofibers by plasma enhanced chemical vapor deposition, using lithographically defined Ni catalyst seeds on TiN. TiN is selected for being an electrically conducting diffusion barrier suitable for the realization of electronic devices. We show that the rate of Ni diffusion correlates to both the level of oxygen content in the TiN film and to the film resistivity. The synthesis of the nanofibers was characterized using electron microscopy with an emphasis on three growth parameters: substrate temperature, plasma power, and chamber pressure. We propose that a catalyst surface free from carbon deposits throughout the process will induce diffusion-limited growth. The growth will shift towards a supply-limited process when the balance between acetylene, as the effective carbon bearing gas, and atomic hydrogen, as the main etching agent, is skewed in favor of acetylene. This determines whether the dominating growth mode will be vertically aligned ‘tip-type’ or disordered ‘base-type’, by affecting the competition between the formation of the first graphitic sheets on the catalyst surface and at the catalyst–substrate interface.

© 2011 Elsevier B.V. All rights reserved.

1. Introduction

The catalytically induced synthesis of vertically aligned carbon nanofibers (VACNFs) by direct current plasma enhanced chemical vapor deposition (dc-PECVD) in which position, diameter, length, and alignment of the nanofibers are accurately determined has offered an unprecedented opportunity to realize new nanoelectromechanical systems (NEMS). Good examples of such devices include the nanoelectromechanical switch [1] and the nanoscale memory cell [2]. In order to expand the boundaries of the VACNF based applications to include those in the radio frequency (rf) range the nanofibers must be grown on top of materials with acceptable performance in that frequency range. Excellent candidates such as copper and gold are not known to yield successful VACNF synthesis. A possible solution is to deposit a thin buffer layer between these materials and the catalyst seeds. Titanium nitride is an efficient diffusion barrier with low electrical resistivity [3] and its compatibility with VACNF synthesis has been demonstrated previously [4]. Another attractive property of TiN is its CMOS compatibility [5] which is an important parameter for future integration [6].

The aim of this work is to explore the growth of VACNFs from Ni catalyst seeds on stoichiometric TiN as a diffusion barrier layer. In contrast to the majority of previous studies where the growth was initiated from a continuous catalyst film, we study the growth from well-defined Ni seeds in sub-100 nm diameter range using hole-mask colloidal lithography. This minimizes the disparities in substrate–catalyst interaction arising from the variation in the interface area among the seeds and therefore enables us to elaborate on the quality (and especially the growth mode) of the VACNFs based on only the synthesis conditions. The growth of VACNFs is characterized with an emphasis on three growth parameters: substrate temperature, plasma power, and chamber pressure. Special attention is paid to the transition of the growth mode from non-aligned carbon nanofibers to well-aligned VACNFs.

Reproducibility is imperative when aiming for VACNF-based device fabrication. Diffusion of the catalyst into the growth underlayer at elevated temperatures modifies the catalyst shape prior to the growth with non-negligible effects on the overall synthesis reproducibility [3]. This was the motivation to investigate the effects of the deposition conditions of the titanium nitride layer on Ni diffusion. We also study the effects that a slight modification on the surface of TiN films would have on the subsequent synthesis of the VACNFs.

* Corresponding author at: Chalmers University of Technology, Department of Microtechnology and Nanoscience, MC2, BioNano Systems Laboratory, SE-412 96 Göteborg, Sweden. Tel.: +46 031 772 10 00; fax: +46 031 772 36 22.
E-mail address: Farzan@chalmers.se (F.A. Ghavanini).

0924-4247/$ – see front matter © 2011 Elsevier B.V. All rights reserved.
doi:10.1016/j.sna.2011.04.036

Please cite this article in press as: F.A. Ghavanini, et al., Controlling the initial phase of PECVD growth of vertically aligned carbon nanofibers on TiN, Sens. Actuators A: Phys. (2011), doi:10.1016/j.sna.2011.04.036

2. Experimental details

2.1. Ti–N film deposition and characterization

Ti–N films were deposited in a reactive sputtering process on top of thermally oxidized silicon chips with an oxide thickness of 400 nm using two commercial dc magnetron sputtering systems. System A (FHR-MS150) was pumped to a base pressure of less than 8×10^{-7} mbar. Ar and N_2 were introduced into the chamber through separate mass flow controllers (MFCs) and the process pressure was controlled by a throttle valve. The system was equipped with an optical emission spectrometer (OES) which monitored the emission intensity from the glow discharge at the wavelength corresponding to Ti (4113 Å). A secondary radio frequency (13.56 MHz) plasma could also be ignited around the substrate. The primary application of the substrate plasma is to perform *in vacuo* substrate cleaning prior to film deposition. However, we employed the substrate plasma during the deposition to impose a substrate bias in order to improve the film quality [7,8]. Sputtering system B (Nordiko 2000) was also equipped with separate MFCs for Ar and N_2 as well as a throttle valve and it was pumped to base pressures of less than 5×10^{-6} mbar. No optical emission spectrometer was installed in system B, and neither was it possible to apply substrate plasma or substrate bias.

Ti–N films were deposited on five chips at each run in both systems. One chip was used for thickness measurement, one was used for resistivity measurements, and three others were used to study the synthesis of VACNFs. The sheet resistance of the deposited films was measured in a four-point-probe measurement setup (CMT-SR2000 N) within 2 min after the chips were exposed to the atmosphere in order to control the level of film oxidation. The film resistivity was then calculated by taking into account the thickness of the deposited film as measured by a surface profiler (Tencor P.15). X-ray photoelectron spectroscopy (XPS) was carried out *ex situ* using monochromatic Al Kα radiation to investigate the film composition. The top 50 Å of the samples were etched using Ar sputtering inside the specimen chamber prior to the measurement to remove surface contamination.

2.2. Colloidal lithography

Hole-mask colloidal lithography [9] was adopted to inexpensively produce Ni catalyst seeds on top of the TiN films. In contrast to the synthesis of VACNFs from a continuous Ni film, this method enables us to study individual VACNF growth from a single catalyst seed; the condition that closely resembles the actual device fabrication. For this purpose a sacrificial polymethyl methacrylate (PMMA) film was spin-coated onto the TiN film and was given a short (5 s) oxygen plasma treatment to improve its hydrophilicity. Water suspended charged polyelectrolyte was pipetted onto the polymer surface to produce a thin adhesive layer. A colloidal solution containing polystyrene (PS) spheres with opposite electrical charge compared to the polyelectrolyte layer was deposited on the surface. The repulsion between the colloids and attraction between the surface and the colloids prevents them from undesirable agglomeration. This is followed by a deionized water rinse and an intense nitrogen blow dry to rapidly remove the solvent and prevent colloidal rearrangement during the drying process (Fig. 1a). 10 nm of gold was then deposited on top of the stack in an electron-beam evaporation equipment (Fig. 1b). After the deposition the PS spheres were stripped away using an adhesive tape leaving nano-scale holes in the thin gold film (Fig. 1c). Reactive oxygen plasma etching was used to remove the PMMA underneath the openings in the gold mask (Fig. 1d). Ni was deposited in the same electron-beam evaporation system at base pressures below 3×10^{-2} mbar. No substrate heating was used during the nickel deposition. The film thickness was controlled during the deposition by a quartz-crystal-based thickness monitor. The colloidal pattern was transferred to the Ti–N substrates in a lift-off process (Fig. 1e and f). Fig. 1g shows a scanning electron microscopy (SEM) image of the resulting Ni seeds on top of the Ti–N. In order to determine the diameter range of the deposited catalyst seeds, micrographs were taken from different areas of a chip at 0° tilt using a calibrated SEM at high magnification. The diameter of the seeds was measured manually. The average diameter was found to be 80 nm and the diameter variation was within ±20 nm.

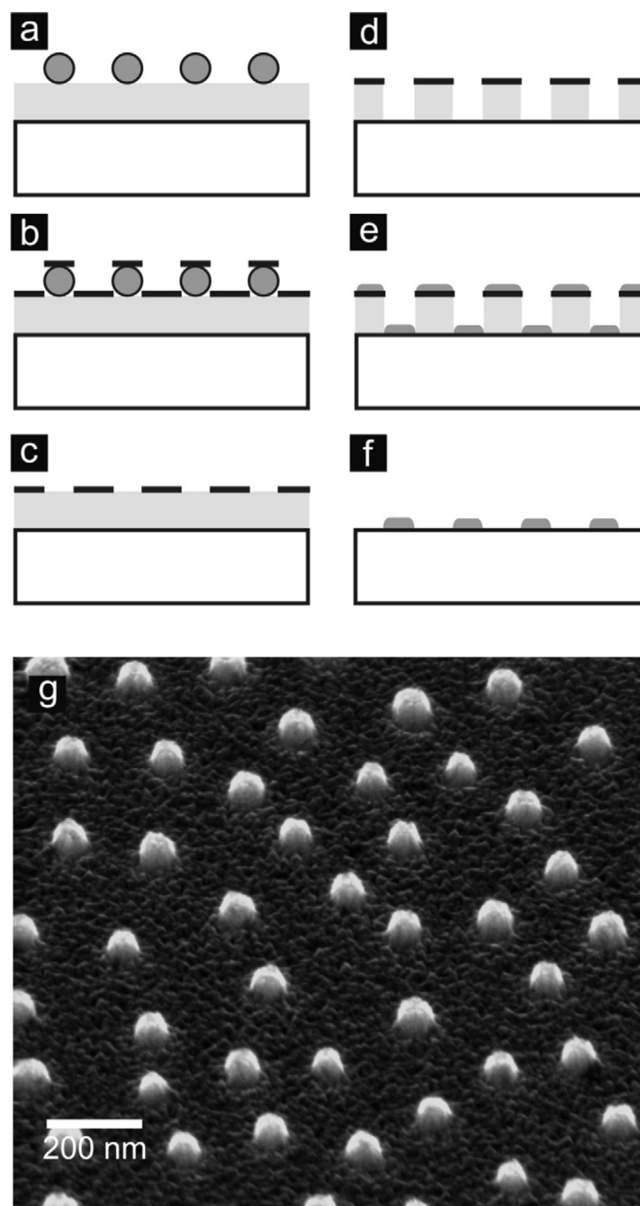

Fig. 1. The schematic illustration of hole-mask colloidal lithography. See text for details. The SEM picture is taken at 40° tilt.

2.3. Oxygen plasma treatments

Oxygen plasma treatments were carried out in a reactive ion etching (RIE) equipment (Plasma Therm Batchtop RIE 95m). Samples were placed on top of a cooled stainless steel substrate. The chamber was pumped and then was filled with oxygen flowing at 10 SCCM (standard cubic centimeter per minute) and the pressure was set to 250 mTorr. Samples were treated separately under

Please cite this article in press as: F.A. Ghavanini, et al., Controlling the initial phase of PECVD growth of vertically aligned carbon nanofibers on TiN, Sens. Actuators A: Phys. (2011), doi:10.1016/j.sna.2011.04.036

capacitively coupled plasma at different powers and for different durations.

2.4. Diffusion tests

Diffusion tests and synthesis of CNFs were both performed in an AIXTRON Black Magic direct current PECVD reactor. The reaction chamber was a bell jar which did not allow base pressures of less than 5×10^{-2} mbar. A fast-response graphite heater capable of providing up to 300 °C per minute ramp rate was used. The samples were loaded directly onto the graphite heater. Process gasses were introduced through separate mass flow controllers and entered the chamber from a showerhead placed directly on top of the heater. The pressure could be controlled by adjusting a leak valve connecting the chamber to the pump line. However, the leak valve was set once and the process pressure was controlled by changing the input gas flow rates.

The diffusion tests were carried out at 4 mbar NH_3 flowing at 160 SCCM. The samples were heated from room temperature to 650 °C at 100 °C per minute. When the target temperature was reached the heater was turned off immediately and the samples were cooled in vacuum.

2.5. Synthesis of VACNFs

The synthesis process adopted in this work can be divided into three main steps: controlled warm-up, plasma treatment, and growth. The controlled warm-up step was carried out in 4 mbar NH_3 during which the temperature was increased by 300 °C per minute from room temperature to 600 °C, unless otherwise stated. The conditions of the warm-up step determine how the catalyst seeds are converted to catalyst nanoparticles [10,11] which directly influences the quality of the subsequent growth. After the warm-up step and while the NH_3 ambiance and the temperature were maintained, the plasma was ignited and the treatment continued for 15 s. The purpose of this step was to chemically reduce the native oxide on the catalyst seeds and therefore enhance the subsequent carbon diffusion during the growth step [12]. Finally, the growth was initiated at the same temperature by introducing acetylene as the carbon containing precursor. The flow rate ratio was 1:4 (C_2H_2:NH_3) in all growth trials. The growth continued for 2 min (5 min in case of oxygen plasma effect study) after which the heater and plasma were turned off and the process chamber was evacuated. The short synthesis time enabled us to study the initial phase of the growth. The samples were cooled in vacuum. The results were analyzed by SEM (Zeiss Supra 60 VP) at 40° tilt. Samples for transmission electron microscopy (TEM, JEOL JEM2100) analysis were prepared by cleaving wedge shape pieces and mounting them onto silver wires (0.25 mm in diameter) using electrically conducting epoxy glue. These were then placed in a TEM holder (from Nanofactory Instruments) and oriented such that the electron beam from the TEM was incident parallel to the Ti–N surface. The TEM instrument was equipped with a digital camera (SC1000) from Gatan, and operated at 100 keV kinetic energy in order to minimize sample damage caused by the electron beam.

2.6. Reproducibility of the growth process

The PECVD synthesis of carbon nanofibers is complex and multidimensional; a large variety of different neutral and charged species are present in a typical growth process which give rise to an even larger set of reactions [13]. The reproducibility in a specific growth chamber depends on how well the density of these species and the rate at which individual reactions are taking place can be controlled. Temperature plays an important role in controlling the above conditions. At the same time, reading the temperature and accurately translating it to the actual temperature of the chip is a formidable task. We found out, through experience, that the inaccuracies in reading and translating the temperature are major sources of irreproducibility. Generally, in low pressure cold-wall CVD chambers such as our growth equipment, heat transport from the heater to the chip laid on top of it is mainly through radiation [14]. Therefore the condition of the heater surface, for example the thickness and the nature of carbon deposits from previous runs (even after a proper cleaning), could potentially modify the efficiency of the heat transfer which is not reflected by the temperature readout. Nevertheless, the main observations given in this work were validated through a large number of growth trials; although the exact result may not be reproduced from the same set of conditions every time the growth process is repeated, the trends reported from modifying any of the three studied growth parameters are completely reproducible.

3. Results and discussion

3.1. Ti–N deposition conditions

Reactive sputtering is a complex process with highly nonlinear behavior and often exhibits hysteresis effects [15]. This makes reproducible deposition of compound films with controlled stoichiometry very challenging. In the case of Ti–N, the stoichiometry of the deposited film is often controlled by adjusting the N_2 partial pressure in the process chamber [16–23]. However, it may be difficult to obtain stable processing conditions using this method. The instability stems from the fact that an incremental increase in the N_2 supply from the optimum value results in an increase in the nitride content formed on the target which has a lower sputtering yield than the metallic Ti. This leads to preferential sputtering of Ti which increases the nitride content of the target even more; a runaway situation develops leading to deposition of non-stoichiometric nitrogen-rich films [16,24,25]. This problem can be avoided if an optical spectrometer is used to monitor, for example, the intensity of the Ti signal which is proportional to the sputtering rate [26]; a change in the intensity level can then be counteracted by readjusting the N_2 supply through a fast responding piezo-valve [3]. However, the piezo-valve was not available in any of the sputtering systems used in this work. Instead, we regulated the magnetron current in response to the change in the emission intensity. The magnetron current is correlated to the density of Ar ions causing the sputtering [27] and provides direct control over the nitride formation on the target surface. This method has been used previously by Berg et al. [16] to deposit stoichiometric TiN films. Yet, the need for dynamic adjustment of the magnetron current during the process is not eliminated unless the process instability is minimized. Kadlec et al. have proposed that if the pumping speed of the system is greater than a critical value then the process instability is completely removed [28,29]. Although reaching the critical pumping speed might be unrealistic in many systems [30], maximizing the pumping throughput nevertheless minimizes the process instability. We adopted this method to deposit Ti–N films in system A where the throttle valve was kept fully open during the process and N_2 and Ar flow rates were fixed at 3 and 92 SCCM, respectively. Fig. 2 shows the intensity of the Ti signal from the optical spectrometer versus the magnetron current for both increasing and decreasing currents. A small hysteresis is still observed at the transition region from metallic Ti to TiN. It is known that the optimum operating point to deposit stoichiometric TiN is at the lower current level in the detected transition region on the increasing-current curve [16] corresponding to 1.9 A magnetron current in Fig. 2. The process was very stable and could easily be reproduced at every operating point. Seven sets of samples were produced, one at each of the magnetron currents from 1.75 A to 2.05 A at 0.05 A steps.

Please cite this article in press as: F.A. Ghavanini, et al., Controlling the initial phase of PECVD growth of vertically aligned carbon nanofibers on TiN, Sens. Actuators A: Phys. (2011), doi:10.1016/j.sna.2011.04.036

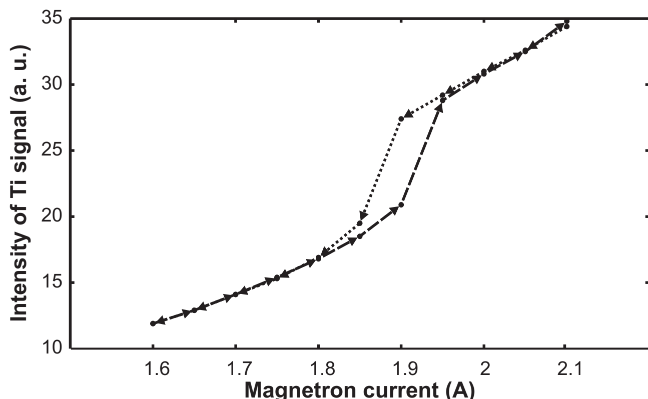

Fig. 2. The intensity of the Ti signal read from the optical emission spectrometer versus the magnetron current for both increasing and decreasing currents.

In system B, Ti–N films were deposited using the conventional method of adjusting N_2 partial pressure. It has been reported that the nitrogen to titanium ratio in the deposited film shows only a minor increase above 2 mol% N_2 in the sputtering gas and reaches unity at about 10 mol% [31]. Since the pumping speed was the same for both Ar and N_2 and the total gettering of the titanium target was rather low in the system (no significant change in the total pressure was observed when the plasma was turned off), the mole percentage provides a direct measure for the gas flow rate ratios. Three sets of samples were fabricated at nitrogen mole percentages of 2, 10 and 50. The chamber pressure was set to 2.5 mTorr in all the runs. Since there was no means to monitor the stability of the process during the deposition, a 5 min pre-deposition was performed while the chips were isolated from the plasma by a shutter to let the system stabilize.

3.2. Film composition analysis by XPS

Fig. 3 shows the XPS spectra of the Ti 2p and the N 1s core levels for the films deposited in both systems. The spectral lines completely overlap for the films deposited in system A at and adjacent to a magnetron current of 1.9 A (optimum point according to Fig. 2). The two prominent peaks at 454.8 eV and 460.8 eV in the Ti 2p spectra are from TiN and the satellite peaks centered at 458.0 eV and 463.9 eV have been attributed to titanium oxynitride TiO_xN_y [18,32]. The N 1s spectra in Fig. 3b exhibits a main peak at 397.3 eV corresponding to on-site nitrogen atoms in a face-centered cubic (fcc) TiN lattice [33]. No significant difference is observed in the elemental fraction of oxygen, nitrogen, and titanium between the three films as shown in Fig. 4a. The discrepancy between titanium and nitrogen content may come from the sputter cleaning process prior to the XPS measurement which preferentially removes N [32]. A cross-section of the TiN film deposited at a magnetron current of 1.9 A is presented in Fig. 5 which clearly shows the expected columnar structure typical of sputtered films [34]. The voids between the columns can enhance the diffusion of oxygen down into the film after exposure to air [35]. This could explain the presence of oxygen in the deposited films.

The spectral lines for the films deposited at 10 mol% and 50 mol% in system B are overlapping as shown in Fig. 3c and d. They are

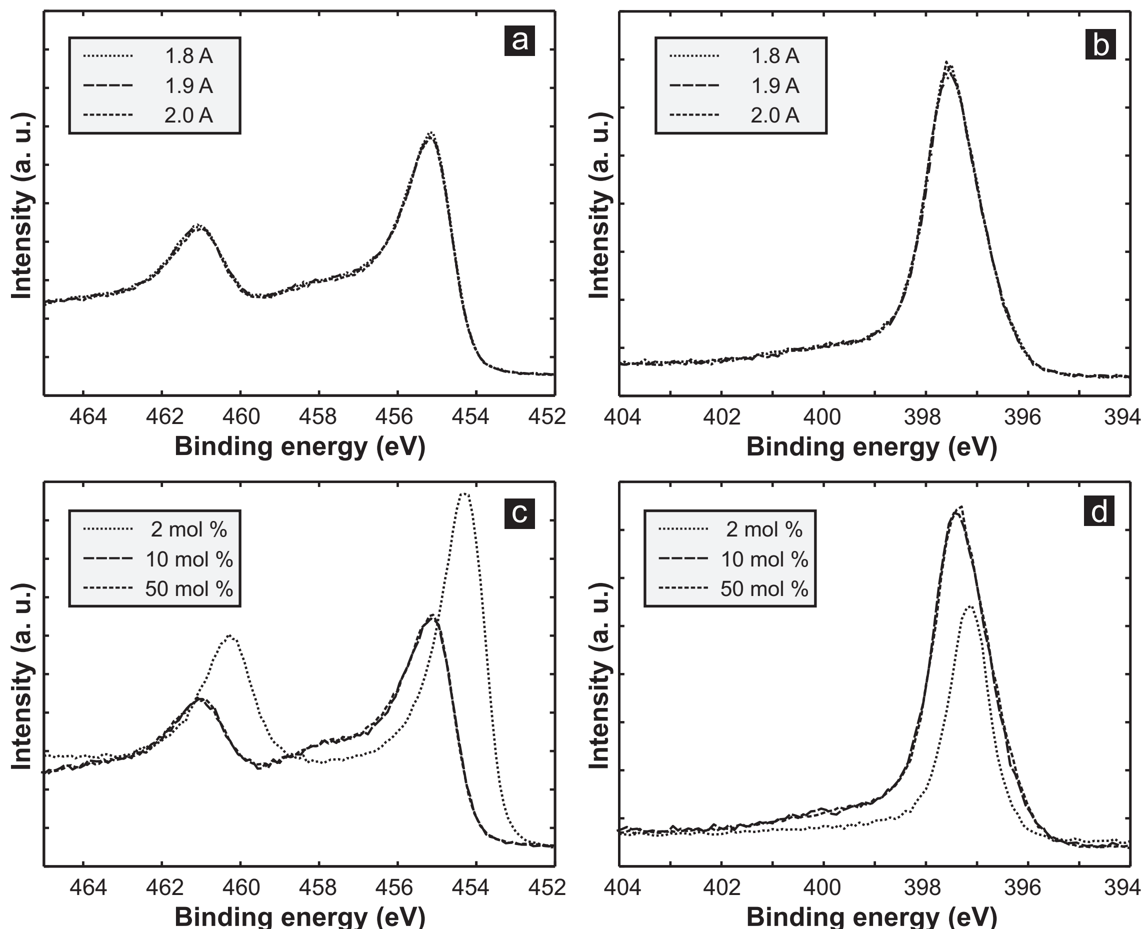

Fig. 3. The XPS spectra of the Ti–N films deposited in (a)–(b) system A and (c)–(d) system B. (a) and (c) show the Ti 2p spectra and (b) and (d) show the N 1s spectra.

Please cite this article in press as: F.A. Ghavanini, et al., Controlling the initial phase of PECVD growth of vertically aligned carbon nanofibers on TiN, Sens. Actuators A: Phys. (2011), doi:10.1016/j.sna.2011.04.036

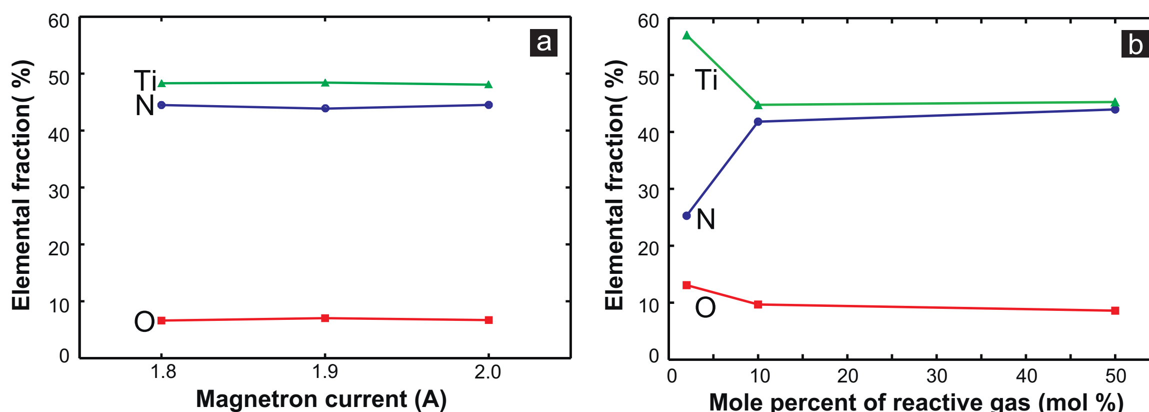

Fig. 4. Elemental analysis from XPS measurements. Fraction of titanium, oxygen, and nitrogen in the Ti–N films deposited (a) in system A as a function of magnetron current and (b) in system B as a function of N_2 partial pressure.

comparable with the XPS spectrum of the films deposited in system A. However, they show more pronounced satellite peaks in the Ti 2P spectra which indicates a higher level of oxygen. This is also evident from the elemental fraction given in Fig. 4b. The Ti 2p spectra of the film deposited at 2 mol% in system B is significantly different from all the other films. Both of the dominant peaks are shifted toward lower binding energies. This shift has been associated with the transition from fcc TiN to hcp (hexagonal closed-pack) Ti saturated with nitrogen [18]. Deviations from stoichiometry as can be seen from Fig. 4b result in a higher degree of vacancies which occur at the nitrogen sublattices for substoichiometric compositions [31,34]. Consequently the oxygen content of the films is dramatically increased.

3.3. Electrical resistivity

The minimum electrical resistivity of Ti–N films, which is lower than that of pure titanium, has been found to occur at a composition corresponding to stoichiometric TiN [5,23]. For single-crystal TiN films values as low as 18 μΩ cm has been reported [36]. The values obtained for single-phase poly-crystal TiN films are not less than 24 μΩ cm [23]. Fig. 6a shows the resistivity of the films deposited in system A at different magnetron currents. In order to exclude the effects that film thickness may have on the resistivity, the same thickness of Ti–N (150 ± 5 nm) was deposited at each magnetron current. The minimum resistivity of 37 μΩ cm was obtained at a magnetron current of 1.9 A corresponding to the optimum operating point in Fig. 2; the lower current level in the transition region. The discrepancy between the minimum reported value for poly-crystal TiN films and the value we obtained here can mainly be attributed to the presence of impurities such as oxygen [8] and the large density of voids located at the grain boundaries [34]. The resistivity values given in Fig. 6a were achieved by setting the substrate plasma to 600 W during the deposition. This imposed a negative bias of 85 V to the substrate through a self-biasing [37] mechanism.

The electrical resistivity of the films deposited in system B is significantly larger than for those fabricated in system A (see Fig. 6b). One may expect more comparable resistivities especially for the films deposited at 10 mol% and 50 mol% because of the similarity in their stoichiometry and oxygen content. We believe that this relatively large difference is due to the application of substrate plasma in system A. It is well known that a negative sub-

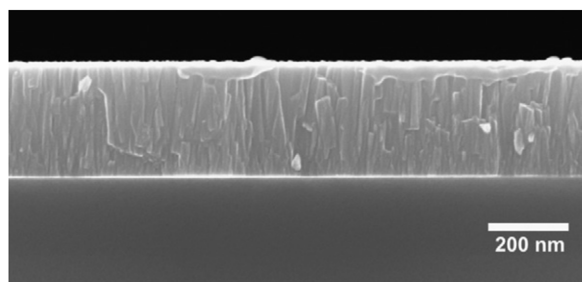

Fig. 5. SEM micrograph showing a cross-section of the Ti–N film deposited in system A at the magnetron current corresponding to 1.9 A.

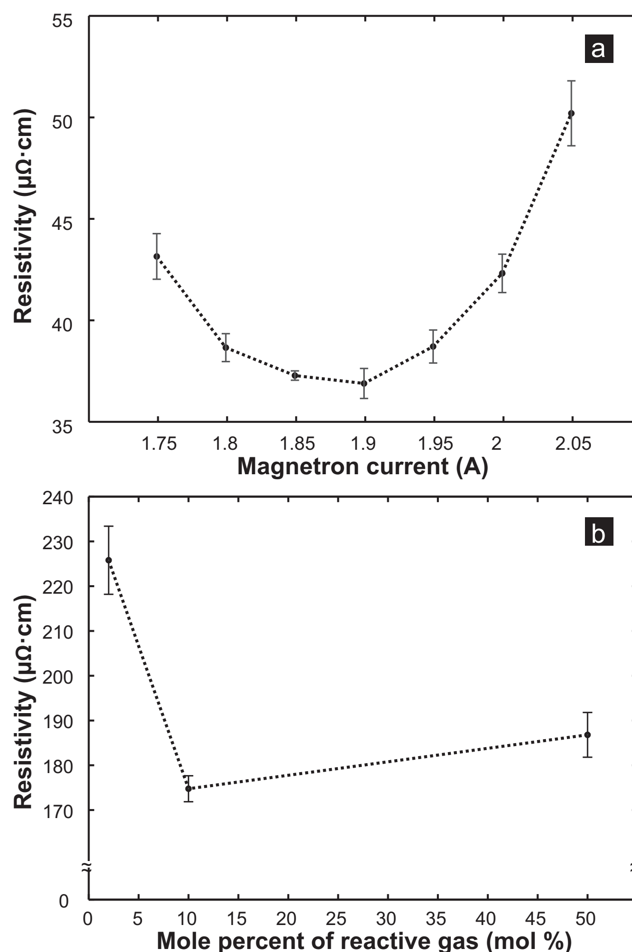

Fig. 6. Electrical resistivity of the Ti–N films deposited in (a) system A as a function of magnetron current and (b) in system B as a function of N_2 partial pressure.

Please cite this article in press as: F.A. Ghavanini, et al., Controlling the initial phase of PECVD growth of vertically aligned carbon nanofibers on TiN, Sens. Actuators A: Phys. (2011), doi:10.1016/j.sna.2011.04.036

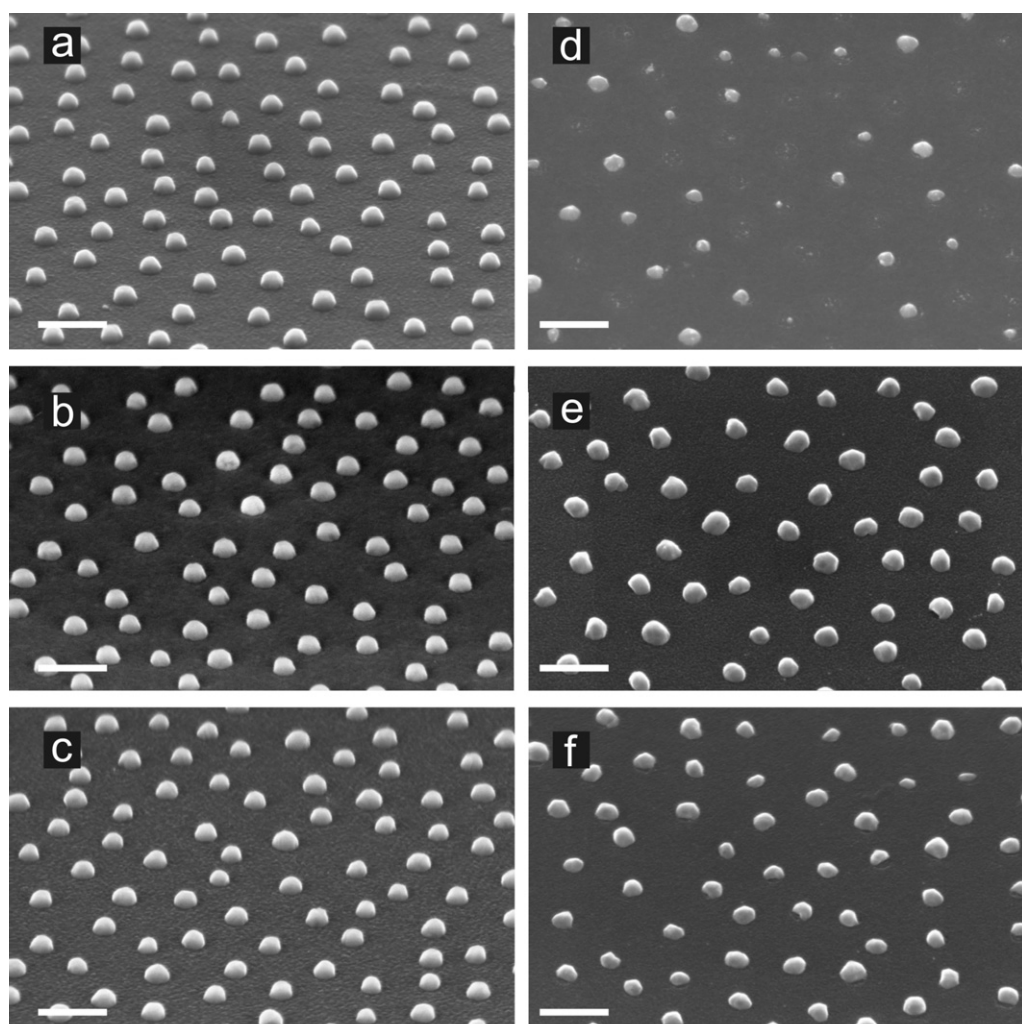

Fig. 7. SEM micrographs showing Ni catalysts on top of different Ti–N films after the diffusion tests. The original thickness of the Ni seeds was 50 nm. (a)–(c) Ti–N films deposited in system A at magnetron current corresponding to (a) 1.8 A, (b) 1.9 A, and (c) 2.0 A. (d)–(f) Ti–N films deposited in system B at N_2 partial pressure corresponding to (d) 2 mol%, (e) 10 mol%, (f) and 50 mol%. The scale bar shows 200 nm. Pictures are taken at 40° tilt.

strate bias affects the microstructure [8,38]. Negative substrate bias decreases the grain size which enhances the electrical conductivity by producing a denser film with a lower density of voids [8,39]. Furthermore, the substrate-bias-induced ion bombardment of the growing film most likely increases the substrate temperature which is also known to reduce the electrical resistivity [40,41].

3.4. Nickel diffusion into Ti–N films

Fig. 7a–c shows the results of the diffusion test on top of the films deposited at 1.8 A, 1.9 A, and 2.0 A in system A, respectively. It can be seen that the seeds have converted to droplet-like nanoparticles, relatively uniform in diameter. In contrast, the catalyst nanoparticles are less uniform and show a wide distribution in their diameter on top of the films deposited in system B as shown in Fig. 7d–f. In particular, they are very small and have even disappeared frequently on top of the film prepared at 2 mol% nitrogen in system B as shown in Fig. 7d suggesting that the diffusion into this film is considerable taking into account the thickness of the nickel seeds before the annealing process which was 50 nm. This is in good agreement with what was observed from the electrical measurements and the XPS analysis: this film has the highest resistivity and the largest oxygen concentration, both indicators of a high density of voids. The same trend is observed in the films deposited at 20 mol% and 50 mol% nitrogen in system B as shown in Fig. 7e and f, respectively. The latter which had shown higher electrical resistivity also presents a larger number of catalyst nanoparticles with reduced diameter after the diffusion test. We did not quantify the Ni diffusion and therefore it was not possible to compare the degree of diffusion among the films deposited in system A. Nonetheless, very similar electrical resistivities and oxygen contents may suggest that they are also very similar in their diffusion characteristics. We repeated the diffusion test on top of TiN films deposited at 1.9 A in system A but with catalyst seeds as thin as 5 nm and 10 nm. The results, as shown in Fig. 8, confirm that the diffusion is indeed negligible since the uniformity of the nanoparticles is preserved although a small decrease in diameter is observed for the chip with 5 nm-thick nickel seeds.

3.5. Synthesis of VACNFs on top of stoichiometric TiN films

3.5.1. Effect of oxygen plasma treatment

Surface oxide is spontaneously formed when as-deposited TiN films come into contact with air [42]. The formation of the oxide layer can be accelerated by exposing the films to an oxygen plasma. Exposure to a mild oxygen plasma for a short period of time (usually referred to as ashing) is a very common surface treatment in a microfabrication processing line. The main purpose of the ashing process is to remove organic contaminations such as polymer residuals after lithography processes. Therefore, one needs to take

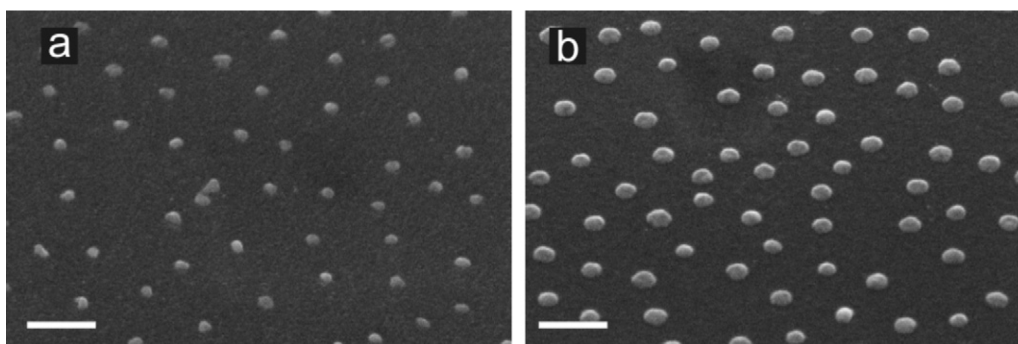

Fig. 8. SEM micrographs taken after the diffusion test was repeated for thinner Ni seeds on top of the TiN films deposited at 1.9 A magnetron current in system A. The original thickness of the Ni catalyst seeds is (a) 5 nm and (b) 10 nm.

into account the consequences of such a surface modification on subsequent growth of VACNFs especially when reproducibility is important. In order to investigate the effect of the surface oxide, we deliberately exposed TiN films to a mild oxygen plasma treatment before depositing the catalyst and compared the quality of the grown VACNFs to that obtained from the growth on top of a pristine TiN film. Since the application of the colloidal lithography would inevitably expose the underlying film to an oxygen plasma step (see Fig. 1d), it was not possible to assess the quality of VACNFs grown from predefined catalyst seeds on top of pristine films. Thus, we studied the effect only on the growth from a continuous catalyst film. Two TiN samples were prepared at 1.9 A magnetron current in system A. One of the samples received a 50 W oxygen plasma treatment for 10 s. Then, 15 nm of nickel was e-beam evaporated on both of the samples in one run. The samples were moved in air to the PECVD reactor and VACNFs were grown at a flow rate of 60:240 (C_2H_2:NH_3) SCCM at a total pressure of 6.45 mbar. The plasma power was set to 80 W and the growth was carried out for 15 min. SEM pictures were taken after the growth from different spots on both chips. The quality of the growth was uniform within each sample. Fig. 9 shows a representative SEM picture from each chip. It is clear that the surface modification imposed by the oxygen plasma treatment has altered the way the catalyst film is broken into nanoparticles resulting in a higher density of nanofibers with reduced diameter (Fig. 9b). At the same time the uniformity in the nanofibers diameter has declined. Although it is not clear why such a trend is observed, the result shows that even a slight surface modification has a pronounced effect on the subsequent synthesis of VACNFs.

3.5.2. *Effect of synthesis parameters*

The effect of synthesis conditions on the growth of VACNFs on top of TiN films deposited in system A at 1.9 A magnetron current were studied. The VACNFs were grown from Ni seeds patterned by colloidal lithography with 15 nm thickness. We particularly studied the effect of three synthesis parameters, namely: substrate temperature, plasma power, and chamber pressure. The effect of each parameter was investigated in a series of three growth processes in which all the growth parameters remained unchanged except for the parameter under the study.

Fig. 10a–c shows the effect of the substrate temperature. In this series, chamber pressure and plasma power were set to 7.0 mbar and 200 W, respectively, while the substrate temperature increased from 600 °C to 650 °C and then to 700 °C. One can see that the growth rate does not increase significantly with the increased temperature. In fact, the derived activation energy (see Fig. 11) was as low as ~0.3 eV. This value is comparable with the activation energy reported by Hofmann et al. (0.23 eV) [43] and Chhowalla et al. (0.5 eV) [10] for PECVD synthesis of carbon nanofibers. The most commonly accepted mechanism for carbon nanotube and nanofiber synthesis by CVD consists of four steps: (1) adsorption of the gas precursor molecules on the catalyst surface, (2) precursor dissociation, (3) diffusion of the growth species in or on the catalyst particle, and (4) nucleation and incorporation of carbon into the growing structure. Since these processes are sequential, the slowest process with the largest energy barrier will be the rate-limiting step. Many authors have identified the diffusion of carbon in or on the catalyst as the rate-limiting step [10,44–48]. If this is the case, then the activation energy for carbon diffusion in our system must be quite low (0.3 eV). In fact, Hofmann et al. [48] have used *ab initio* density functional calculations to show that the barrier for carbon diffusion on the Ni(1 1 1) surface is as low as 0.4 eV. This agrees well with our TEM observations revealing that in the majority of the VACNFs the catalyst particle has been oriented along the [1 1 0] direction with {1 1 1} planes exposed to the plasma (see Fig. 12). Thus, the low activation energy for the growth is explained by a low energy barrier surface diffusion mechanism. Another important observation in Fig. 10a–c is the pronounced etching effect

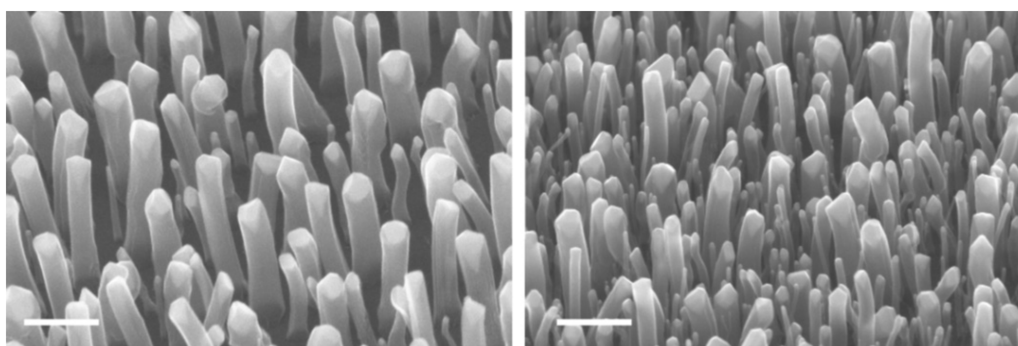

Fig. 9. Effect of oxygen plasma treatment on the subsequent growth of VACNFs; SEM micrographs of VACNFs grown on top of (a) a pristine TiN film, (b) a TiN film exposed to 10 s oxygen plasma at 50 W, and (c) a TiN film exposed to 60 s oxygen plasma at 100 W. The scale bar shows 500 nm.

Please cite this article in press as: F.A. Ghavanini, et al., Controlling the initial phase of PECVD growth of vertically aligned carbon nanofibers on TiN, Sens. Actuators A: Phys. (2011), doi:10.1016/j.sna.2011.04.036

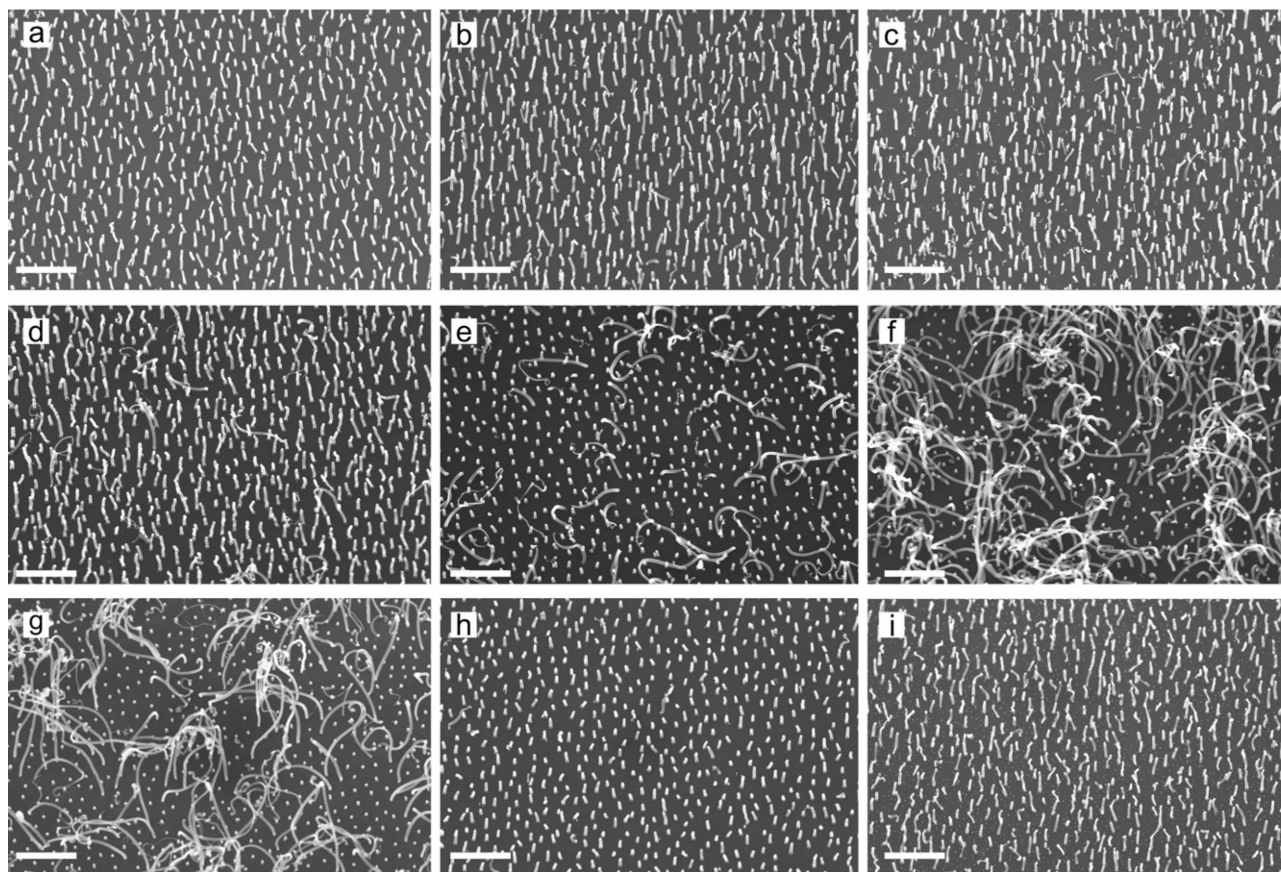

Fig. 10. Effect of synthesis conditions on the growth of VACNFs; (a)–(c) temperatures effect: VACNFs grown at 7.0 mbar, 60:240 (C_2H_2:NH_3) SCCM, 200 W plasma power, and substrate temperature of (a) 600 °C, (b) 650 °C, and (c) 700 °C. (d)–(f) Effect of chamber pressure: VACNFs grown at 600 °C, plasma power of 120 W, and C_2H_2:NH_3 gas ratio of 1:4 at a total pressure of (d) 3.3 mbar, (e) 9.7 mbar, (f) 10.2 mbar. (g)–(i) Effect of plasma power: VACNFs grown at 600 °C, 30:120 (C_2H_2:NH_3) SCCM for a total pressure of 4.6 mbar, and a plasma power of (g) 60 W, (h) 120 W, (i) 200 W. In all cases, the growth was carried out for 2 min. The scale bar shows 1 μm.

resulting from using a relatively high plasma power (200 W) which has lead to defective nanofibers. This also implies that no carbon deposits have formed on the exposed surfaces of the Ni catalysts throughout the growth process.

The effect of chamber pressure is shown in Fig. 10d–f. In this series, the substrate temperature and the plasma power were fixed at 600 °C and 120 W, respectively. The chamber pressure was increased from 3.3 mbar to 9.7 mbar and then to 10.2 mbar. It can be seen that the increase in the chamber pressure has decreased the growth rate of the aligned nanofibers while it has given rise to the growth of non-aligned carbon nanofibers (see Fig. 10f). It is well known that the vertical alignment of the nanofibers depends on the position of the catalyst seed relative to the growing structure [49–52]. In a ‘tip-type’ growth where the catalyst is located at the tip, vertical alignment is achieved while in a ‘base-type’ growth where the catalyst seed remains on the substrate no ver-

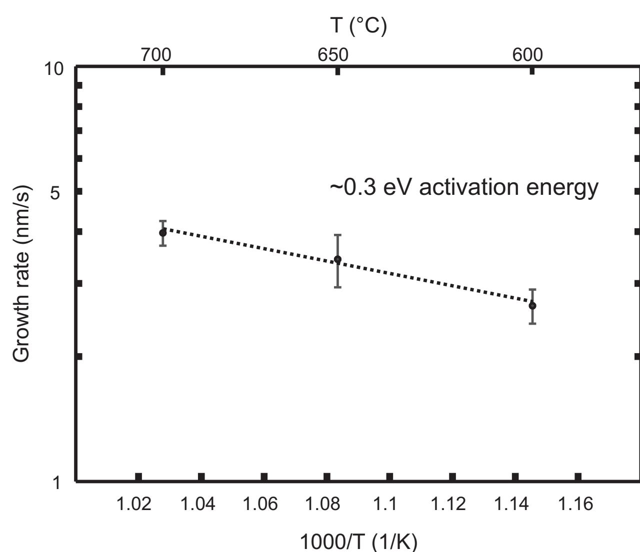

Fig. 11. The change in the growth rate versus the substrate temperature. The value for the activation energy was calculated from a linear interpolation.

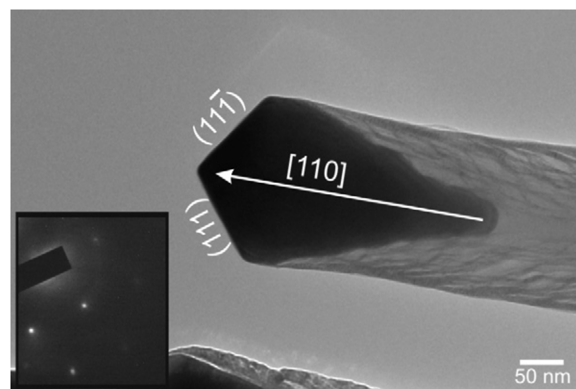

Fig. 12. A TEM image of a typical VACNF grown in the synthesis study. The catalyst at tip of the VACNF is oriented along the [1 1 0] direction with two {1 1 1} planes exposed to the plasma. The inset shows selected area diffraction from the catalyst in the TEM image.

Please cite this article in press as: F.A. Ghavanini, et al., Controlling the initial phase of PECVD growth of vertically aligned carbon nanofibers on TiN, Sens. Actuators A: Phys. (2011), doi:10.1016/j.sna.2011.04.036

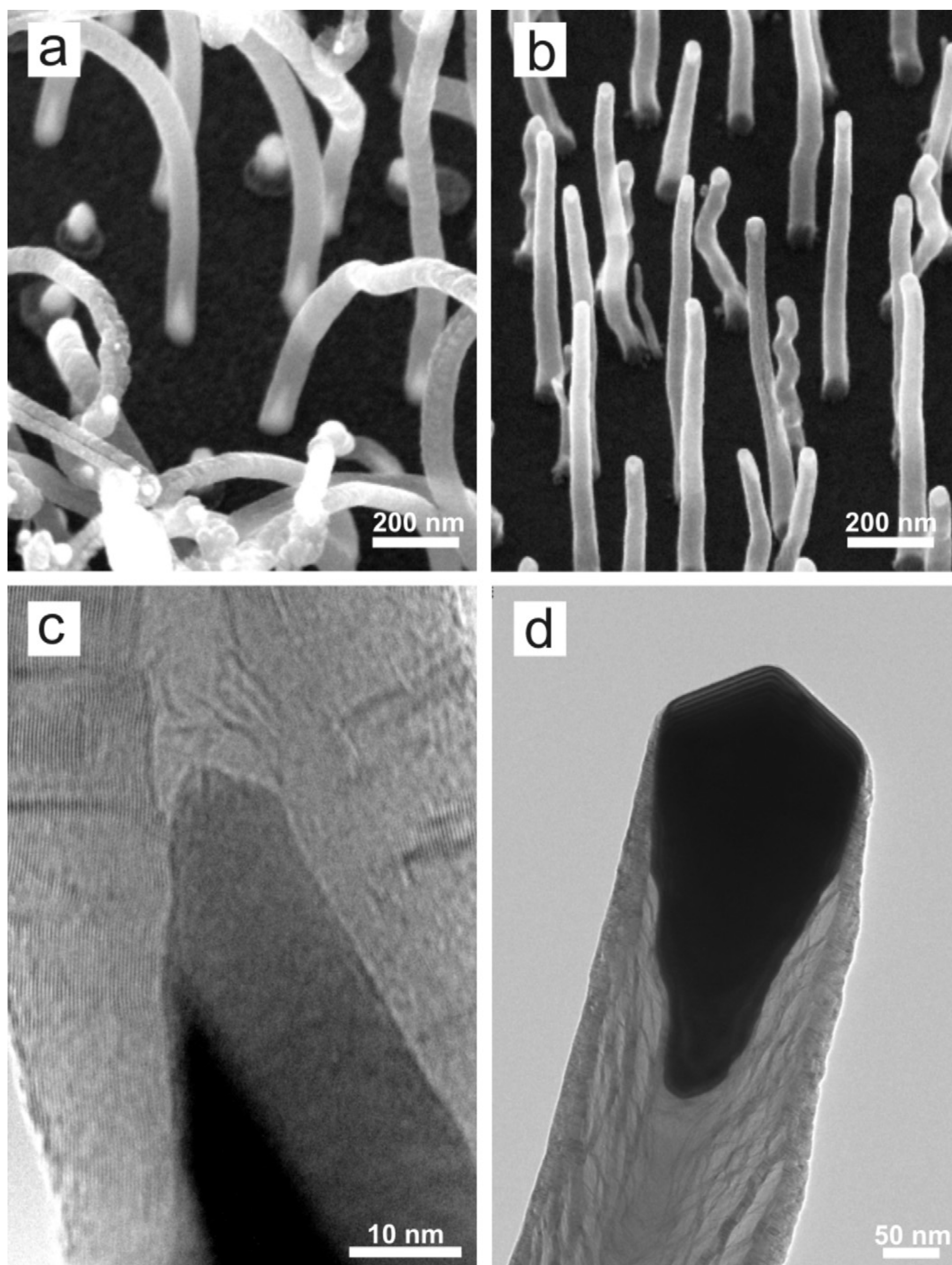

Fig. 13. Internal structure of the synthesized nanofibers. (a) and (b) show SEM images of base-type and tip-type carbon nanofibers, respectively; the catalyst nanoparticles are clearly visible due to their higher contrast. TEM images of base-type (c) and tip-type (d) carbon nanofibers reveal conically shaped stacks of graphene.

tical alignment is obtained [53]. A closer look at the syntheisezed nanofibers reveals this fact. Fig. 13a and b shows SEM micrographs of nonaligned and aligned nanofibers, respectively, where the catalyst seeds are clearly visible at the bottom and at the tip of the nanofibers. Their internal structures are shown by TEM images in Fig. 13c and d. Although both types are made of stacked graphene sheets with a non-zero angel between the sheets and the fiber axis, the base-type nanofibers (see Fig. 13c) present a denser and more uniform structure with smaller cone angels. The transition between the growth modes has been attributed to different parameters. Song et al. [50] among others [46,54] have suggested that the interaction between the catalyst and the substrate defines the growth mode, that is, a weak interaction leads to the 'tip-type' and a strong interaction gives the 'base-type' growth. However, in our case, these interactions should not differ significantly from one catalyst seed to another especially since the substrate–catalyst interface area is relatively constant among all of them. Pre-growth processing variations cannot be accounted for the observed growth mode transition either given that all the chips were fabricated in one batch. A more plausible reason for the transition observed here, as suggested by Melechko et al. [49], could be the change in the growth conditions. The increased pressure has produced 'tip-type' nanofibers, as shown in Fig. 10e and f, which are considerably shorter than what was achieved at the same temperature (600 °C) in the previous series (see Fig. 10a). This suggests that another step in the process than the carbon diffusion has taken over as the rate-limiting step. We believe that the increased pressure has shifted the growth to a supply-limited state where the arrival or the decomposition of

Please cite this article in press as: F.A. Ghavanini, et al., Controlling the initial phase of PECVD growth of vertically aligned carbon nanofibers on TiN, Sens. Actuators A: Phys. (2011), doi:10.1016/j.sna.2011.04.036

the carbon bearing species is now the rate-limiting step. The two carbon bearing gasses with the highest densities in a C_2H_2/NH_3 plasma are acetylene and hydrogen cyanide (HCN) [55]. It has been shown that acetylene is the main precursor for growth of carbon nanofibers with Ni as the catalyst [55,56]. At the lowest pressure the plasma power of 120 W is large enough to create the necessary density of atomic hydrogen by dissociating ammonia and acetylene [13]. This generates a balance between acetylene as the effective carbon bearing gas and atomic hydrogen as the main etching agent keeping the exposed catalyst facets free of carbon deposits throughout the growth process. As long as the catalyst surface is 'clean' the growth dynamics remains in a diffusion-limited state. This can explain the similarity of the VACNFs length in Fig. 10d to those in Fig. 10a–c. Increasing the chamber pressure increases the population of acetylene molecules. Consequently, the balance is skewed in favor of acetylene. The main result of such a shift is an increased probability for the formation of carbon islands on the catalyst surface. The average area of the catalyst surface covered by the carbon patches will then depend on how far the balance is distorted in favor of C_2H_2. This phenomenon has also been mentioned by Merkulov et al. [57] and Gohier et al. [58]. They argued that the change in the catalyst active area changes the rate at which acetylene is decomposed at the catalyst surface and thereby changes the growth rate. This is in complete agreement with our observations in this work.

The same argument can be used to explain the transition in the growth mode. The transition occurs when a continuous carbon cap forms on the catalyst surface which impedes the carbon diffusion from the surface. However, this carbon cap must form before the 'tip-mode' growth has commenced, that is, before the first graphene layers have formed on the catalyst–substrate interface. In other words, the growth mode transition can be explained in terms of a competition between the formation of the first graphitic sheets on the catalyst surface and on the catalyst–substrate interface; whichever forms first will decide the growth mode. It is more likely that a continuous carbon film forms on the catalyst exposed surfaces when the etching process is not efficient. That is why the increase in the population of the 'base-type' nanofibers coincides with a decline in the 'tip-type' growth rate. However, it remains for further investigation to determine why the 'base-type' nanofibers exhibit a much higher growth rate.

The plasma power effect is shown in Fig. 10g–i. In this series, the substrate temperature and the chamber pressure were fixed at 600 °C and 4.6 mbar, respectively. The plasma power was increased from 60 W to 120 W and then to 200 W. The observed trend agrees well with the model developed in the last paragraph. Increasing the plasma power increases the dissociation rate and creates more radicals including the etching agents. Therefore the catalyst surface remains 'cleaner' during the process at larger plasma powers and therefore a higher growth rate is yielded. Again, we can see that the maximum growth rate (achieved at the largest plasma power) is comparable to the rate for the diffusion-limited case. We note that our results differ from those obtained by Bell et al. [59] where a decrease in the growth rate was observed by increasing the power. They argued that the increased gas-phase acetylene decomposition at higher plasma powers limits the carbon supply bearing in mind that acetylene is the most effective growth precursor in the plasma. In the same work, residual gas analysis (RGA) was used to show that there is an optimum point at around 23% acetylene (percentage of acetylene in total C_2H_2 plus NH_3) where the concentration of H_2 which is generated by the decomposition of both NH_3 and C_2H_2 is the minimum. Both at higher and at lower acetylene concentrations the amount of H_2 increased. They argued that at acetylene concentrations lower than the optimum value, H_2 is mainly generated from NH_3 decomposition while at the concentrations larger than 23% acetylene is decomposed preferentially over NH_3. We believe this could explain the disagreement between the result obtained in this work and those obtained by Bell et al. if we assume that at our growth conditions ammonia is decomposed preferentially. Therefore an increase in the plasma power does not modify the acetylene concentration significantly but only produces more etching agents. The growth conditions in the work by Bell et al. on the other hand favor the acetylene decomposition over NH_3 and therefore increased plasma power reduces the concentration of acetylene and hence reduces the growth rate.

4. Conclusions

We present a reliable method to deposit stoichiometric TiN films by adjusting the magnetron current in a reactive sputtering process. We achieved a minimum electrical resistivity of 37 $\mu\Omega$ cm by employing the substrate plasma during the film deposition. We show that the diffusion of Ni into the TiN films is negligible when the deposition is done with the application of the substrate plasma. The diffusion was considerable in the films deposited without the substrate plasma although their stoichiometries were not significantly different. The higher rate of Ni diffusion coincided with a higher level of oxygen content in the films and larger electrical resistivity. These observations emphasize the importance of the film microstructure in determining the rate of diffusion. This can be manipulated to a large extent by parameters such as the substrate plasma. We also show that slight surface modifications such as the formation of a surface oxide imposed by a light plasma ashing alters the subsequent growth of VACNFs.

The synthesis of VACNFs on top of stoichiometric TiN films was characterized with an emphasis on three growth parameters: substrate temperature, plasma power, and chamber pressure. We argue that if the catalyst surface remains free of carbon deposits throughout the process the growth stays in a diffusion-limited state. We found that the activation energy for nanofiber growth is quite low (~0.3 eV) which could be explained by a surface diffusion rate limiting mechanism. We show that the growth shifts to a supply-limited state when the balance between acetylene as the effective carbon bearing gas and atomic hydrogen as the main etching agent is skewed in favor of acetylene.

Finally, by excluding the catalyst-size dependencies through patterning Ni into well-defined seeds we were able to explain the transition in the growth mode based on a competition mechanism; if the first graphitic sheets form on the exposed surface of the catalyst a 'tip-type' growth initiates while if these sheets are formed first on the catalyst–substrate interface the growth mode will be of 'base-type'.

References

[1] J.E. Jang, S.N. Cha, Y. Choi, G.A.J. Amaratunga, D.J. Kang, D.G. Hasko, J.E. Jung, J.M. Kim, Nanoelectromechanical switches with vertically aligned carbon nanotubes, Applied Physics Letters 87 (2005) 263103.
[2] J.E. Jang, S.N. Cha, Y.J. Choi, D.J. Kang, T.P. Butler, D.G. Hasko, J.E. Jung, J.M. Kim, G.A.J. Amaratunga, Nanoscale memory cell based on a nanoelectromechanical switched capacitor, Nature Nanotechnology 3 (2008) 26–30.
[3] J. Garcia-Cespedes, J. Alvarez-Garcia, X. Zhang, J. Hampshire, E. Bertran, Optimal deposition conditions of TiN barrier layers for the growth of vertically aligned carbon nanotubes onto metallic substrates, Journal of Physics D: Applied Physics 42 (2009).
[4] K.B.K. Teo, M. Chhowalla, G.A.J. Amaratunga, W.I. Milne, G. Pirio, P. Legagneux, F. Wyczisk, D. Pribat, D.G. Hasko, Field emission from dense, sparse, and patterned arrays of carbon nanofibers, Applied Physics Letters 80 (2002) 2011–2013.
[5] M. Wittmer, H. Melchior, Applications of TiN thin-films in silicon device technology, Thin Solid Films 93 (1982) 397–405.
[6] F.A. Ghavanini, H. Le Poche, J. Berg, A.M. Saleem, M.S. Kabir, P. Lundgren, P. Enoksson, Compatibility assessment of CVD growth of carbon nanofibers on bulk CMOS devices, Nano Letters 8 (2008) 2437–2441.
[7] J.E. Sundgren, B.O. Johansson, S.E. Karlsson, Influence of substrate bias on composition and structure of reactively r.f.-sputtered TiC films, Thin Solid Films 80 (1981) 77–83.

Please cite this article in press as: F.A. Ghavanini, et al., Controlling the initial phase of PECVD growth of vertically aligned carbon nanofibers on TiN, Sens. Actuators A: Phys. (2011), doi:10.1016/j.sna.2011.04.036

[8] J.M. Poitevin, G. Lemperiere, J. Tardy, Influence of substrate bias on the composition, structure and electrical properties of reactively d.c.-sputtered TiN films, Thin Solid Films 97 (1982) 69–77.
[9] H. Fredriksson, Y. Alaverdyan, A. Dmitriev, C. Langhammer, D.S. Sutherland, M. Zaech, B. Kasemo, Hole-mask colloidal lithography, Advanced Materials 19 (2007) 4297.
[10] M. Chhowalla, K.B.K. Teo, C. Ducati, N.L. Rupesinghe, G.A.J. Amaratunga, A.C. Ferrari, D. Roy, J. Robertson, W.I. Milne, Growth process conditions of vertically aligned carbon nanotubes using plasma enhanced chemical vapor deposition, Journal of Applied Physics 90 (2001) 5308–5317.
[11] M.S. Bell, K.B.K. Teo, W.I. Milne, Factors determining properties of multi-walled carbon nanotubes/fibres deposited by PECVD, Journal of Physics D: Applied Physics 40 (2007) 2285–2292.
[12] S.J. Randolph, J.D. Fowlkes, A.V. Melechko, K.L. Klein, H.M. Meyer, M.L. Simpson, P.D. Rack, Controlling thin film structure for the dewetting of catalyst nanoparticle arrays for subsequent carbon nanofiber growth, Nanotechnology 18 (2007).
[13] K.B.K. Teo, D.B. Hash, R.G. Lacerda, N.L. Rupesinghe, M.S. Bell, S.H. Dalal, D. Bose, T.R. Govindan, B.A. Cruden, M. Chhowalla, G.A.J. Amaratunga, J.M. Meyyappan, W.I. Milne, The significance of plasma heating in carbon nanotube and nanofiber growth, Nano Letters 4 (2004) 921–926.
[14] A. Hasper, J.E.J. Schmitz, J. Holleman, J.F. Verwey, Heat-transport in cold-wall single-wafer low-pressure chemical-vapor-deposition reactors, Journal of Vacuum Science and Technology A: Vacuum Surfaces and Films 10 (1992) 3193–3202.
[15] T. Larsson, H.O. Blom, C. Nender, S. Berg, A physical model for eliminating instabilities in reactive sputtering, Journal of Vacuum Science and Technology A: Vacuum Surfaces and Films 6 (1988) 1832–1836.
[16] S. Berg, T. Larsson, H.O. Blom, The use of nitrogen flow as a deposition rate control in reactive sputtering, Journal of Vacuum Science and Technology A: Vacuum Surfaces and Films 4 (1986) 594–597.
[17] H.O. Blom, S. Berg, T. Larsson, Mass-flow limitations in reactive sputtering, Thin Solid Films 130 (1985) 307–313.
[18] M. Delfino, J.A. Fair, D. Hodul, X-ray photoemission spectra of reactively sputtered tin, Journal of Applied Physics 71 (1992) 6079–6085.
[19] M.K. Hibbs, J.E. Sundgren, B.E. Jacobson, B.O. Johansson, The microstructure of reactively sputtered Ti–N films, Thin Solid Films 107 (1983) 149–157.
[20] J. Musil, L. Bárdos, A. Rajský, J. Vyskocil, B. Dolezal, G. Loncar, K. Dadourek, V. Kubícek, TiNx coatings prepared by d.c. reactive magnetron sputtering, Thin Solid Films 136 (1986) 229–239.
[21] F. Richter, H. Kupfer, H. Giegengack, G. Schaarschmidt, F. Scholze, F. Elstner, G. Hecht, Fundamental mechanisms of titanium nitride formation by dc magnetron sputtering, Surface and Coatings Technology 54 (1992) 338–342.
[22] J.E. Sundgren, B.O. Johansson, S.E. Karlsson, Kinetics of nitride formation on titanium targets during reactive sputtering, Surface Science 128 (1983) 265–280.
[23] J.E. Sundgren, B.O. Johansson, S.E. Karlsson, H.T.G. Hentzell, Mechanisms of reactive sputtering of titanium nitride and titanium carbide. 2. Morphology and structure, Thin Solid Films 105 (1983) 367–384.
[24] S. Berg, H.O. Blom, T. Larsson, C. Nender, Modeling of reactive sputtering of compound materials, Journal of Vacuum Science and Technology A: Vacuum Surfaces and Films 5 (1987) 202–207.
[25] S. Berg, T. Larsson, C. Nender, H.O. Blom, Predicting thin-film stoichiometry in reactive sputtering, Journal of Applied Physics 63 (1988) 887–891.
[26] K.D. Leedy, J.M. Rigsbee, Development of an optical-emission spectroscopy-based method for dynamic compositional analysis of sputter-deposited films from multicomponent targets, Applied Physics Letters 66 (1995) 676–678.
[27] K. Laing, J. Hampshire, D. Teer, G. Chester, The effect of ion current density on the adhesion and structure of coatings deposited by magnetron sputter ion plating, Surface and Coatings Technology 112 (1999) 177–180.
[28] S. Kadlec, J. Musil, H. Vyskocil, Hysteresis effect in reactive sputtering – a problem of system stability, Journal of Physics D: Applied Physics 19 (1986) L187–L190.
[29] S. Kadlec, J. Musil, J. Vyskocil, Influence of the pumping speed on the hysteresis effect in the reactive sputtering of thin-films, Vacuum 37 (1987) 729–738.
[30] T. Nyberg, S. Berg, U. Helmersson, K. Hartig, Eliminating the hysteresis effect for reactive sputtering processes, Applied Physics Letters 86 (2005).
[31] J.E. Sundgren, B.O. Johansson, S.E. Karlsson, Mechanisms of reactive sputtering of titanium nitride and titanium carbide. 1. Influence of process parameters on film composition, Thin Solid Films 105 (1983) 353–366.
[32] A.S. Ingason, F. Magnus, J.S. Agustsson, S. Olafsson, J.T. Gudmundsson, In situ electrical characterization of ultrathin TiN films grown by reactive dc magnetron sputtering on SiO_2, Thin Solid Films 517 (2009) 6731–6736.
[33] E.C. Onyiriuka, Aluminum, titanium boride, and nitride films sputter-deposited from multicomponent alloy targets studied by XPS, Applied Spectroscopy 47 (1993) 35–37.
[34] J.E. Sundgren, Structure and properties of TiN coatings, Thin Solid Films 128 (1985) 21–44.
[35] C. Ernsberger, J. Nickerson, T. Smith, Low-temperature oxidation behavior of reactively sputtered tin by X-ray photoelectron-spectroscopy and contact resistance measurements, Journal of Vacuum Science and Technology A: Vacuum Surfaces and Films 4 (1986) 2784–2788.
[36] B.O. Johansson, J.E. Sundgren, J.E. Greene, A. Rockett, S.A. Barnett, Growth and properties of single-crystal tin films deposited by reactive magnetron sputtering, Journal of Vacuum Science and Technology A: Vacuum Surfaces and Films 3 (1985) 303–307.
[37] J.H. Kim, Y.H. Shin, K.H. Chung, Study on self-bias voltage induced on the substrate by r.f. bias power in a high density plasma, Thin Solid Films 435 (2003) 288–292.
[38] J.E. Sundgren, B.O. Johansson, H.T.G. Hentzell, S.E. Karlsson, Mechanisms of reactive sputtering of titanium nitride and titanium carbide.3. Influence of substrate bias on composition and structure, Thin Solid Films 105 (1983) 385–393.
[39] M.K. Hibbs, B.O. Johansson, J.E. Sundgren, U. Helmersson, Effects of substrate-temperature and substrate material on the structure of reactively sputtered tin films, Thin Solid Films 122 (1984) 115–129.
[40] J.A. Fair, M. Delfino, A comparison of Ti films sputtered in an N-2 Ar plasma at 25-degrees-C and 500-degrees-C, Applied Surface Science 53 (1991) 206–211.
[41] W. Tsai, M. Delfino, J.A. Fair, D. Hodul, Temperature-dependence of the electrical-resistivity of reactively sputtered tin films, Journal of Applied Physics 73 (1993) 4462–4467.
[42] F. Esaka, K. Furuya, H. Shimada, M. Imamura, N. Matsubayashi, H. Sato, A. Nishijima, A. Kawana, H. Ichimura, T. Kikuchi, Comparison of surface oxidation of titanium nitride and chromium nitride films studied by X-ray absorption and photoelectron spectroscopy, Journal of Vacuum Science and Technology A: Vacuum Surfaces and Films 15 (1997) 2521–2528.
[43] S. Hofmann, B. Kleinsorge, C. Ducati, A.C. Ferrari, J. Robertson, Low-temperature plasma enhanced chemical vapour deposition of carbon nanotubes, Diamond and Related Materials 13 (2004) 1171–1176.
[44] F. Abild-Pedersen, J.K. Norskov, J.R. Rostrup-Nielsen, J. Sehested, S. Helveg, Mechanisms for catalytic carbon nanofiber growth studied by ab initio density functional theory calculations, Physical Review B 73 (2006).
[45] S. Helveg, C. Lopez-Cartes, J. Sehested, P.L. Hansen, B.S. Clausen, J.R. Rostrup-Nielsen, F. Abild-Pedersen, J.K. Norskov, Atomic-scale imaging of carbon nanofibre growth, Nature 427 (2004) 426–429.
[46] R.T.K. Baker, Catalytic growth of carbon filaments, Carbon 27 (1989) 315–323.
[47] R.T.K. Baker, M.A. Barber, R.J. Waite, P.S. Harris, F.S. Feates, Nucleation and growth of carbon deposits from nickel catalyzed decomposition of acetylene, Journal of Catalysis 26 (1972), 51-&.
[48] S. Hofmann, G. Csanyi, A.C. Ferrari, M.C. Payne, J. Robertson, Surface diffusion: the low activation energy path for nanotube growth, Physical Review Letters 95 (2005).
[49] A.V. Melechko, V.I. Merkulov, D.H. Lowndes, M.A. Guillorn, M.L. Simpson, Transition between ‘base’ and ‘tip’ carbon nanofiber growth modes, Chemical Physics Letters 356 (2002) 527–533.
[50] I.K. Song, Y.S. Cho, G.S. Choi, J.B. Park, D.J. Kim, The growth mode change in carbon nanotube synthesis in plasma-enhanced chemical vapor deposition, Diamond and Related Materials 13 (2004) 1210–1213.
[51] M. Meyyappan, L. Delzeit, A. Cassell, D. Hash, Carbon nanotube growth by PECVD: a review, Plasma Sources, Science and Technology 12 (2003) 205–216.
[52] A.V. Melechko, R. Desikan, T.E. McKnight, K.L. Klein, P.D. Rack, Synthesis of vertically aligned carbon nanofibres for interfacing with live systems, Journal of Physics D: Applied Physics 42 (2009) 193001–193028.
[53] V.I. Merkulov, A.V. Melechko, M.A. Guillorn, D.H. Lowndes, M.L. Simpson, Alignment mechanism of carbon nanofibers produced by plasma-enhanced chemical-vapor deposition, Applied Physics Letters 79 (2001) 2970–2972.
[54] A.V. Melechko, V.I. Merkulov, T.E. McKnight, M.A. Guillorn, K.L. Klein, D.H. Lowndes, M.L. Simpson, Vertically aligned carbon nanofibers and related structures: controlled synthesis and directed assembly, Journal of Applied Physics 97 (2005) 39.
[55] D.B. Hash, M.S. Bell, K.B.K. Teo, B.A. Cruden, W.I. Milne, M. Meyyappan, An investigation of plasma chemistry for dc plasma enhanced chemical vapour deposition of carbon nanotubes and nanofibres, Nanotechnology 16 (2005) 925–930.
[56] M. Jonsson, O.A. Nerushev, E.E.B. Campbell, Dc plasma-enhanced chemical vapour deposition growth of carbon nanotubes and nanofibres: in situ spectroscopy and plasma current dependence, Applied Physics A: Materials Science and Processing 88 (2007) 261–267.
[57] V.I. Merkulov, D.K. Hensley, A.V. Melechko, M.A. Guillorn, D.H. Lowndes, M.L. Simpson, Control mechanisms for the growth of isolated vertically aligned carbon nanofibers, Journal of Physical Chemistry B 106 (2002) 10570–10577.
[58] A. Gohier, C.P. Ewels, T.M. Minea, M.A. Djouadi, Carbon nanotube growth mechanism switches from tip- to base-growth with decreasing catalyst particle size, Carbon 46 (2008) 1331–1338.
[59] M.S. Bell, K.B.K. Teo, R.G. Lacerda, W.I. Milne, D.B. Hash, M. Meyyappan, Carbon nanotubes by plasma-enhanced chemical vapor deposition, Pure and Applied Chemistry 78 (2006) 1117–1125.

Biographies

Farzan A. Ghavanini has received his B.Sc. degree in electrical engineering in 2004 from K. N. Toosi University of Technology, Tehran, Iran. He obtained his M.Sc. degree in 2006 from Chalmers University of Technology during which he studied design, fabrication, and measurement of microelectromechanical systems (MEMS). His master thesis was on wafer-level encapsulation of MEMS sensors using low-temperature co-fired ceramic (LTCC). He is currently pursuing a Ph.D. at the Department of Microtechnology and Nanoscience at Chalmers University of Technology. His main research interest is the synthesis of vertically aligned carbon nanofibers for nano-electromechanical device applications.

Please cite this article in press as: F.A. Ghavanini, et al., Controlling the initial phase of PECVD growth of vertically aligned carbon nanofibers on TiN, Sens. Actuators A: Phys. (2011), doi:10.1016/j.sna.2011.04.036

Maria Lopez-Damian received her B.Sc. degree in Mechatronics Engineering from Instituto Tecnológico y de Estudios Superiores de Monterrey, México, in 2005. She is currently a graduate student at the Bionano System Laboratory at the Department of Microtechnology and Nanoscience, Chalmers University of Technology, Gothenburg, Sweden. Her main interest is the synthesis of vertically aligned carbon nanofibers for device applications.

Damon Rafieian Boroujeni received his B.Sc. degree in Electronics Engineering from Azad University of Technology, Karaj, in 2006. He received his M.Sc. from Bionano Systems Laboratory at the department of Microtechnology and Nanoscience, Chalmers University of Technology and he is currently a prospective Ph.D student at Twente Univesity, Enschede, Netherlands. His main interest is electrical characterization and optimization of reactively sputtered TiN thin films for the growth of vertically aligned carbon nanofibers.

Krister Svensson obtained a Ph.D. in Physics in 1997 at Chalmers University of Technology, Gothenburg. After a Postdoc in Birmingham, England, during 1998–2000, he worked as a researcher at Chalmers from 2000 to 2007. He now holds a Lecture ship in Physics at Karlstad University. His research interests evolve mainly around fundamental properties of nanostructured materials, such as carbon nanotubes and silicon nanowires. He has done pioneering work on combining scanning probe techniques with electron microscopes, which enables a new range of experiments to be performed inside electron microscopes. He holds several patents in relation to these new instruments.

Per Lundgren has a position as Associate Professor at the Department of Microtechnology and Nanoscience at Chalmers University of Technology. He graduated as a Ph.D. from Chalmers in 1996 on a thesis on electrical characterization of ultrathin oxide layers in metal-oxide-silicon devices. His current academic are focused on undergraduate and graduate education and the solid state electronics research he conducts today relates to heterogeneous integration of novel nanostructured devices in silicon based electronics.

Peter Enoksson received the M.Sc. degree in Engineering Physics in 1986. After a period of work he returned to academia and got the Licentiate of Engineering in 1995 and the Ph.D. in 1997 all from the Royal Institute of Technology, Stockholm, Sweden. In December 1997 he became assistant professor and in 2000 was appointed associate professor at the Royal Institute of Technology, where he was a supervisor and project leader in the Microsystem Technology group. He has also taken a very active part in developing and giving courses in Microsystems and Measurement systems technology. Peter Enoksson was appointed Professor of MOEMS (Micro Opto Electro Mechanical Systems) in 2001 at Chalmers University of Technology, Gothenburg Sweden. In 2002 he was appointed vice dean of School of Electrical Engineering and in 2003 also head of the Solid State Electronics Laboratory, both at Chalmers University of Technology. Currently he heads the Micro- and Nanosystems group at the department of Microtechnology and Nanoscience. His main research activities are in combining MEMS/NEMS with other sciences in building more dedicated and advanced systems. Prof. Enoksson has published more than 150 research journal and conference papers, have three granted and three patents pending. He is one of initiator of two spin-off companies.